2024-12

Synthesis and Characterization of Clay-Supported Cuo Nanocompositef For Degradation of Malachite Green

Getu, Worku

BAHIR DAR UNIVERSITY

COLLEGE OF SCIENCE POST GRADUATE PROGRAM

DEPARTMENT OF CHEMISTRY

SYNTHESIS AND CHARACTERIZATION OF CLAY-SUPPORTED CuO NANOCOMPOSITE FOR DEGRADATION OF MALACHITE GREEN

BY:

GETU WORKU WUDU

ADVISOR: ALEBEL NIBRET (PhD)

CO-ADVISOR: BELETE ASEFA (PhD)

DECEMBER, 2024

BAHIR DAR, ETHIOPIA

Bahir Dar University
College of Science
Department of Chemistry
Postgraduate Program

Synthesis and Characterization of Clay-supported CuO Nanocomposite for Degradation of Malachite Green

BY
Getu Worku Wudu

A thesis submitted to the College of Science, Bahir-Dar University, in Partial Fulfillment of the Requirement for the Degree of Master of Science in Chemistry

Advisor: Alebel Nibret (PhD)
Co-Advisor: Belete Asefa (PhD)

December, 2024
Bahir Dar, Ethiopia

DEDECLARATION

This is to certify that the thesis **"Synthesis and Characterization of Clay-Supported CuO Nanocomposite for Degradation of Malachite Green"** was submitted in partial fulfillment of the requirements for the award of the degree of Master of Science in Chemistry, Department of Chemistry, Bahir Dar University, is a record of original work carried out by me and has never been submitted to this or any other institution to get any other degree or certificates.

Name of the Candidate	**Signature**	**Date**
Getu Worku Wudu	_____	13 December 2024

Bahir Dar University

College of Science Postgraduate Program

Department of Chemistry

Approval of Thesis for Defense

As the research advisor, we now certify that we have supervised, read, and evaluated this thesis entitled: **"Synthesis and Characterization of Clay-supported CuO Nanocomposite for Degradation of Malachite Green"** by Getu Worku Wudu prepared, under our guidance. We recommended that the thesis requirement be submitted for oral defense.

We recommended that it be submitted as fulfilling the MSc thesis requirement.

Alebel Nibret (PhD)	_____	13 December 2024
Advisor	**Signature**	**Date**
Belete Asefa (PhD)	_____	13 December 2024
Co-Advisor	**Signature**	**Date**
Yonas Beyene (PhD)	_____	13 December 2024
Department Head	**Signature**	**Date**

Bahir Dar University

College of Science

Department of Chemistry

Approval of Thesis for Defense Result

As members of the board of examiners of the Master of Sciences (MSc) thesis open defense examination, we have read and evaluated this thesis prepared by Getu Worku entitled **"Synthesis and Characterization of Clay-supported CuO Nanocomposite for Degradation of Malachite Green"**. We now certify that the thesis is accepted for fulfilling the requirements for the award of the degree of Master of Sciences in Chemistry (Physical Chemistry).

Board of Examiners

Name	**Signature**	**Date**
External Examiner _____	_____	_____
Internal Examiner _____	_____	_____
Chairman _____	_____	_____

ACKNOWLEDGMENT

First of all, I would like to thank Almighty God for giving me the strength, knowledge, ability, and opportunity to undertake this research study and to persevere and complete it satisfactorily, without his blessings, this achievement would not have been possible.

I want to express my deepest gratitude to my supervisors, Dr. Alebel Nibret and Dr. Belete Asefa, for their excellent guidance, fruitful comments, suggestions, and consistent supervision throughout my period of study at Bahir Dar University, Department of Chemistry, in every phase of this research work that made it possible to materialize. Their ability to inspire and stimulate chemistry study has made the difference between a dream and reality.

My sincere thanks go to Bahir Dar University, College of Science Department of Chemistry, for their financial support, enabling me to prosper and conduct this research easily. My thanks also go to the staff members who helped and contributed to me during this research work. This study's successful and timely accomplishment would have been difficult without their cooperation.

I am very pleased to thank the head of the chemistry department and other staff members of the chemistry of Bahir Dar University, for hosting me to pursue my MSc degree.

I gratefully acknowledge help from the following organizations: Bahir Dar University, the Department of Biology, and Bahir Dar Institute of Technology (BiT), for providing instruments with a full laboratory facility. Last, but not least, I am also thankful to all of my family and friends for their love and encouragement throughout.

TABLE OF CONTENTS

Contents **Page**

LIST OF TABLES

Tables **Page**

LIST OF FIGURES

Figure **Page**

ABBREVIATIONS

BDU	Bahir Dar University
FTIR	Fourier Transform Infrared Spectroscopy
MSB	Magnetic Susceptibility Balance
NPs	Nanoparticles
NCPs	Nanocomposites
NMs	Nanomaterials
SEM	Scanning Electron Microscopy
US EPA	Environmental Protection Agency
UV-Vis	Ultraviolet-Visible Spectroscopy
WHO	World Health Organization
XRD	X-Ray Diffraction
EDX	Energy Dispersive X-ray spectroscopy
TEM	Transmission Electron Microscopy
BET	Brunauer-Emmett-Teller
MG	Malachite Green
CuO	Copper Oxide
AOP	Advanced Oxidation Process
T-O-T	Tetrahedral Octahedral Tetrahedral

ABSTRACT

Recently, many types of research in clay-based nanocomposites have been accomplished to eliminate pollutants from water sources. Nanocomposite materials have advanced properties useful for contaminate removal such as higher surface area, thermal stability, selectivity to remove different contaminants, improved processability, and fast decontamination. This study aimed to verify the efficiency of heterogeneous photocatalysis for the degradation of organic pollutants. In this work we describe a simple and low-cost method for decolorizing malachite green dye wastewaters, using clay-supported CuO NCPs as a photocatalyst. This nanocomposite was synthesized by the co-precipitation method by stirring at 70 °C using copper pentahydrated salt as a precursor. UV-Vis spectrometer (UV-Vis), Fourier transform infrared spectrometer (FTIR), X-ray diffraction (XRD), scanning electron microscopy along with Energy Dispersive X-ray spectroscopy (SEM-EDX) were investigated to study materials absorbance, functional group, crystalline size, morphology, and elemental analysis respectively. Photocatalytic degradation of aqueous solution of malachite green dye using as-synthesized photocatalysts was studied under a tungsten bulb light. The higher photocatalytic degradation efficiency of clay-supported CuO NCPs is attributed to the increase in the surface area of a composite and the lower rate of recombination of the photo-generated electrons. The percentage degradation efficiency of malachite green dye was 89.67 using 0.064g of clay-supported CuO NCPs and 20 ppm malachite green dye aqueous solution at a contact time of 180 minutes.

Keywords: *As-synthesized photocatalysts, clay, co-precipitation method, decolorization, malachite green dye.*

CHAPTER ONE

1. INTRODUCTION

1.1. Background of the Study

Nanotechnology plays an important function in recent environmental aspects for the elimination of contaminants in the ecosystem. Recently, nano-clay has initiated more concentration because of its distinctive physicochemical properties and characteristics. Organic dyes are used by a wide range of businesses and professions, such as textiles, leather, plastic sheets, medicine, cosmetics, and nutrition, to color their products and discharge their waste into the environment without any care [1, 2]. Due to their stability against oxidizing agents, it is not a simple method to extract from the dye-containing wastewater. The aquatic ecosystem and human health are at risk from these vibrant organic contaminants [3, 4]. These coloring substances slow down the photosynthetic process in the aquatic environment, block sunlight from entering water streams, and may combine with ionic metals to produce chelating complexes, which can harm living things [5]. Malachite (MG) is among the numerous organic dyes found in wastewater. It is a triphenylmethane cationic green dye employed as a parasiticide in the fishing industry and as a coloring agent for leather, textile, and woolen products. But even at low doses (1 mg L^{-1}), MG can cause cancer and have a major negative impact on human health [6]. It is therefore crucial that it be removed from industrial waste before being released into the environment, which encourages scientists to create an affordable and practical wastewater treatment method. The creation of an efficient nano-sized photocatalyst has attracted a lot of attention in this regard [7].

Powdered semiconductors have recently gained a lot of attention for their possible degradation capacity in the presence of light energy when used as catalysts in the photodegradation of several organic pollutants. Researchers developed a variety of physical, chemical, and advanced treatment methods, including membrane filtration, ion exchange, electrochemical technology, coagulation, flocculation, reverse osmosis, chemical oxidation, ozonation, and biological treatment for the effects of bacteria and fungi, to remove dye from wastewater [8]. The majority of these systems, however, have several drawbacks, including poor efficiency, high energy consumption, high cost, non-selectivity, unsuitability for large-scale applications, and the production of hazardous secondary sludge [9]. Semiconductor nanomaterials are currently

commonly used in the removal of different organic dyes under visible light illumination using a sophisticated oxidation process via heterogeneous photocatalysis. This approach is inexpensive, simplifies catalyst manufacturing, and has high dye removal efficiency [10]. During this process, extremely reactive free radicals were produced, which caused the organic chemicals in the wastewater to break down into innocuous products like CO_2, H_2O, and other byproducts when semiconductors were exposed to the right kind of artificial or natural light source [11]. Organic contaminants, like dye deposited on the semiconductor surface, may completely degrade as a result of the intricate chain of events triggered by the produced electron/hole pairs [12]. To eliminate organic dyes from the wastewater industry, some methods have been developed [13–15]. The metal oxide semiconductor-assisted photocatalytic process is one of the more popular methods for reducing aqueous organic dyes because of its exceptional qualities, which include cheap cost, direct use of free solar energy, reusability, and the absence of additional unwanted chemicals [16, 17]. The primary causes of photocatalytic activity in metal oxide nanocomposites are the catalyst's electrical structure, band gap, and shape. When compared to homogeneous catalysts, the usage of solid catalysts such as metal and metal oxide nanoparticle support materials performed better. This is mostly because of the catalysts' capacity to withstand harsh conditions and be recycled and reused.

Transition metal oxides are interesting photocatalysts because of their easier synthesis and ability to form different metal-oxygen ratios, due to their half-filled d orbitals that enable them to form different oxidation states, with varying properties and catalytic pollutants removal performance [18]. Copper (II) oxide is a transition metal oxide that has numerous applications in different fields. To maximize pollutant eradication, the bandgap should not be too small (<1.3 eV) to minimize the high probability of charge carriers recombination nor be too large (>3.0 eV) to be activated in the visible region of the electromagnetic spectrum and as such a band gap in the range of 1.3 3.0 eV has generally been reported to be appropriate for photocatalytic degradation.
It is an intrinsically p-type semiconductor owing to oxygen vacancy defects in its crystal structure and has an indirect narrow bulk bandgap of 1.2 eV. Copper (I) oxide or cuprous oxide (Cu_2O) and copper (III) oxide (Cu_4O_3) are other polymorphs and while Cu_2O is a thermally less stable phase than CuO, Cu_4O_3 is a metastable phase with a mixed oxidation state of Cu atom and is difficult to synthesize [19]. CuO nanostructures are interesting to researchers in the photocatalytic eradication of pollutants from wastewater [20]. However, fast charge carrier

recombination and a low specific surface area hinder its efficiency and widespread application in photocatalysis. Because of the high probability of photogenerated e−/h+ pairs recombination which suppresses the photonic and hence its removal efficiency. Nanomaterials physicochemical properties are strictly dependent on their size and morphology. Hence, improving some of the surface morphological properties of CuO by coupling hetero junction semiconductor supportive materials via an improved synthetic route increases the rate of photocatalytic degradation activities. By facilitating charge transfer across heterojunctions and inducing additional photocatalytic activity, these interfacial states can effectively improve the separation of photo-generated electron-hole pairs [21].

To support CuO NPs, solid supports are crucial because they function as ligands and shields from reactive and uncontrollable environments. They can also help by offering an active surface location, which directly increases reactivity. Regretfully, most support materials are quite expensive, and the synthesis processes are challenging and time-consuming. Nonetheless, locally available clay minerals have attracted a lot of interest as nanoparticle substrates due to their intrinsic, financial, and ecological qualities, including their high surface area, excellent adsorption, and cation-exchange capability. Because of their consistent morphology and eco-friendly qualities, clay minerals are regarded as potential supporting materials [22, 23]. Although silica, alumina, magnesium, or both, and water make up the majority of clay minerals, iron may also replace aluminum and magnesium to varied degrees, and significant amounts of potassium, sodium, and calcium are also commonly found. Due to its unique surface characteristics, including a huge surface area, good stability, and a very hydrophilic surface, this material has been used extensively to build functional nanoparticles [24]. Using clay compounds as support materials is one of the most economical methods to create nanoparticles. This is because clay compounds are less costly than other support materials, such as graphene and carbon nanotubes, which are more costly than cheap clay [25]. Consequently, the degradation of MG dyes was investigated using clay-supported CuO NCPs produced by the co-precipitation process.

1.2. The problem of the study

The increasing number of industries worldwide tends to be the main reason for water pollution, and the production of synthetic dyes is increasing due to their high demand, especially in the textile and clothing industries. Organic, inorganic, and biological toxins can seriously harm a

person's physical or nervous system when they are present in their drinking water and food source. This study focused on the synthesis of semiconductor nanomaterials for the application of photocatalytic degradation of organic pollutants in wastewater. Metal oxide semiconductors are the most often studied materials in photocatalysis owing to their high photocatalytic activity, nontoxicity, and chemical stability [26]. Among different metal oxides, a well-known metal oxide photocatalyst is CuO, which has demonstrated usefulness in many photocatalytic applications including hydrogen generation, water treatment, and air purification. However, fast charge carrier recombination and a low specific surface area along with utilized operational parameters are prominent drawbacks that hinder its efficiency and widespread application in photocatalysis. A high massive photogenerated electron-hole recombination limits the efficiency of the photocatalyst. Inhibiting the chance of photogenerated e^-/h^+ pairs recombination of CuO can be alleviated via a certain supportive to control its morphology and size or coupling it with other semiconductors with proper band gap alignment to form heterojunctions [27]. Unfortunately, the majority of support materials are excessively costly, and the procedures involved in synthesis are difficult and time-consuming. However, cost-effective locally available clay nanomaterials play important roles in supporting metal oxide nanoparticles, by positioning themselves as ligands and protectors for reactive and uncontrolled conditions; these can contribute to providing an active surface site which contributes directly to the reactivity. As compared to conventional wastewater treatment techniques, heterogeneous photocatalysis is a preferable option owing to its advantages such as ease of application, less costly as only a small amount of catalyst and light may be used to run the degradation reactions, which can proceed at ambient conditions, environmentally friendly, and involves the elimination of pollutants rather than transferring them from one phase to another as in the case of adsorption [28].

1.3. Significance of the study

The significance of this study lies in its potential to contribute to the development of eco-friendly and sustainable methods for the synthesis of clay-supported CuO NPs. It is believed that the results of this research can provide useful information for the design of a better semiconductor that would combine the ability to dissociate dye molecules with a high surface area that absorbs light while retaining high stability. The result of the study had an important effect on the design and use of such nanocomposites and conveyed important information about the activity of clay-

supported CuO NCPs toward the photodegradation of pollutants in wastewater. By addressing critical areas, this study has the potential to make meaningful contributions to both science and society, emphasizing the importance of innovative material solutions for pressing environmental challenges.

1.4. Objective of the study

1. 4.1. General Objective

To synthesize, characterize, and evaluate the photocatalytic activity of clay-supported CuO nano-composite for malachite green (MG) dye degradation.

1.4.2. Specific Objective

- ✓ To synthesize clay-supported CuO NCPs.
- ✓ To characterize as-synthesized CuO NPs and clay-supported CuO NCPs by XRD, SEM-EDX, FTIR, and UV–Vis techniques
- ✓ To examine the photocatalytic degradation efficiency of as-synthesized photocatalysts for degradation of MG dye.

CHAPTER TWO

2. LITERATURE REVIEW

2.1. Historical aspects and growth of nanoscience and nanotechnology

The word nano originates from the Greek word dwarf, which typically describes a particle that is between one and one hundred nanometers in size. Richard Feynman's 1959 presentation introduced the theoretical idea of nanotechnology; he made conjectures on the potential and possibilities of materials at the nanoscale [20]. Nanotechnology was initially coined by Norio Taniguchi of Tokyo Science University in 1974. Nanotechnology was then abbreviated as Nanotech. It wasn't until the early 1990s, nevertheless, that nanotechnology took off. Early in the 1990s, Huffman and Kretschmer figured out how to make and purify large amounts of fullerenes, which are molecules made entirely of carbon that resemble graphite in structure. Graphite is made up of a sheet of linked hexagonal rings, but fullerenes have pentagonal (or occasionally heptagonal) rings that keep the sheet from being flat. The discovery and characterization of carbon nanotubes was presented by T. Ebbesen to an enthralled audience shortly after a 1992 Materials Research Society meeting. Nanotechnology was advanced by hundreds of researchers using the same or comparable instruments as Huffman and Kretschmer. How many items on the market now are made using nanotechnologies or include nanoparticles is unknown [29]. The study of designing, creating, modifying, and using materials with nanometer-scale dimensions, or nanomaterials, is known as nanotechnology [30]. It involves using science to manipulate matter at the molecular level [29]. In all disciplines, including chemistry, biology, physics, material science, and engineering, it is also the study and usage of little objects [31]. Numerous scholars from the aforementioned domains have expressed interest in it [32]. Nanotechnology often works with nanoparticles, which are structures that range in size from 1 to 100 nm. It entails creating objects or materials in that range of sizes [29]. Nanobiotechnology, bionanotechnology, quantum dots, Surface-enhanced Raman Scattering (SERS), and applied microbiology are just a few of the new basic and applied frontiers in materials science and engineering that have been made possible by the tremendous expansion of nanotechnology [33]. Almost every aspect of civilization, including communications, computing, textiles, cosmetics, sports, therapy, automobiles, environmental monitoring, fuel cells and energy devices, water purification, the food and beverage industry, etc., could be impacted by this truly

multidisciplinary and emerging field of nanoscience and technology [29]. Our understanding of matter is being revolutionized by nanoscience and nanotechnologies, which will likely have a significant impact on every area of the economy, including food and agriculture, energy production and efficiency, the automobile industry, cosmetics, medical devices and medications, household appliances, computers, and weapons. Our ability to prevent, detect, and remove environmental toxins from soil, water, and air in an economical and ecologically responsible way might be enhanced by nanotechnology [29].

2.2. Nanoparticles or nanomaterials

When compared to the bulk material, NPs, which are solid particles having all three exterior dimensions at the nanoscale, can significantly alter the physicochemical characteristics. Materials with at least one exterior dimension in the range of roughly 1 to 100 nm are referred to as NMs. At the nanoscale, this is frequently not the case, whereas bulk materials have very consistent physical characteristics regardless of their size. The nanoparticles have special optical, biological, and physicochemical characteristics that may be appropriately adjusted for the intended uses [29]. In contrast to conventional and commercial bulk materials, they have special electrical, magnetic, optical, catalytic, and therapeutic qualities. This is because of its huge surface-to-volume ratio, quantum size effect, and discrete electronic energy states [34]. The characteristics of particles can vary significantly when they are shrunk from micrometers to nanometers. For instance, it is known that changes can occur in electrical conductivity, hardness, active surface area, chemical reactivity, and biological activity [35]. Because the surface of the material dominates the bulk characteristics, this might result in surprising properties of nanoparticles. The characteristics of materials are known to alter as their dimensions are reduced to the atomic level.

The surface area-to-volume ratios of all nanoparticles are quite high, irrespective of their chemical composition. Because of this, the surface atoms and capping agents have a greater influence on the physical characteristics of the nanoparticles. High surface area particles have more reaction sites than low surface area particles, which leads to enhanced chemical reactivity. For applications like catalysis, a high surface area to volume ratio is crucial. Nature frequently makes use of this heightened responsiveness caused by the surface area to volume ratio; the

digestive system of the body is one biological example. Millions of folds and subfolds make up the small intestine, increasing the surface area of the digestive tract's inner lining. The efficiency of our body and the speed at which we digest food is significantly increased by these folds, which enable the simultaneous absorption of more nutrients and substances. Another example might be a sugar cube interacting with water, where the sugar's exterior is dissolved. A sugar cube of uniform size is divided into several little fragments. Every incision creates a fresh surface on which the water may dissolve.

The smaller sugar particles have a substantially larger surface area but the same volume. Nanoparticles have a lot of intriguing characteristics because of their minuscule size and vast surface area. Electronics, optoelectronics, magnetics, information storage, recording media, sensing devices, catalysis, chemistry, environment, energy, agriculture, medicine and drug delivery, communication technology, aircraft technology, heavy industry, and consumer goods are among the fields in which they find new uses as a result. Because of their distinct chemical and physical characteristics, nanomaterials have seen a sharp rise in attention in recent years [33]. It is also clear that the unique chemical and physical properties of nanomaterials such as diffusivity, electrical resistivity, electrical conductivity, strength and hardness, chemical reactivity, and diverse and versatile biological activity that set them apart from their bulk counterparts have led to an exponential increase in research interest in these materials [30]. Since they exhibit entirely new or improved properties based on particular characteristics like size, shape, distribution, ionic strength, capping agent, and morphology, nanoparticles are of great interest because they serve as a bridge between the atomic/molecular structure and the material in bulk. Additionally, their size, shape, and structure have a significant impact on their prospective uses [31]. Material science has been significantly impacted by nanoparticles. Due to the basic and technological significance of the ongoing research on this subject, it appears that this supremacy will persist in the years to come. With uses across several industrial sectors, nanoparticles are regarded as the fundamental components of the next generation of technology [30]. In general, the nanoparticles are divided into two categories: inorganic and organic. Because of their resistance to unfavorable processing conditions, the latter have become more important.

2.3. Nanocomposites

Nanocomposites are known as the result of binding two different components in a nanoscale with distinctive physical and chemical behavior. Binding various materials not only integrates their properties but also produces a new effect and decreases the limitation features of the single species. The composite nanoparticles have significant application prospects in some major industrial fields, such as manufacturing new functional materials, utilizing a new source of energy effectively, remediating wastewater, and introducing new applications in the biomedicine and food industries [35].

2.4. Semiconductors

Solids, in general, possess different band gaps which result in diverse properties. Based on varying bandwidths, they are classified as metals, insulators, and semiconductors. Solids (like metals), have overlapped band gaps regardless of the temperature. The higher band is the conduction band whereas the lower one is the valence band and possesses a gap for semiconductors and insulators. The band gap in insulators is very high; hence, it is difficult to excite electrons from the valence to the conduction band, which is called the forbidden gap. However, in semiconductors, the band gap is small enough for the electrons to move from the valence to the conduction band at room temperature as shown in Figure 1 below. Their bandgap ranges from 0 to 7 eV bounding energy levels in visible and UV light [35]. Photocatalysis involves light irradiation on the catalyst which functions as thermal energy and hence excites the electron from the valence to the conduction band of the catalyst. Therefore, the band gap's width is the primary requisite for an efficient photocatalyst, which strongly influences the electrical and optical characteristics of the material. To utilize the light from the solar spectrum or light bulb band gap engineering is the fundamental approach operated for semiconducting materials, and hence they are broadly utilized as photocatalysts.

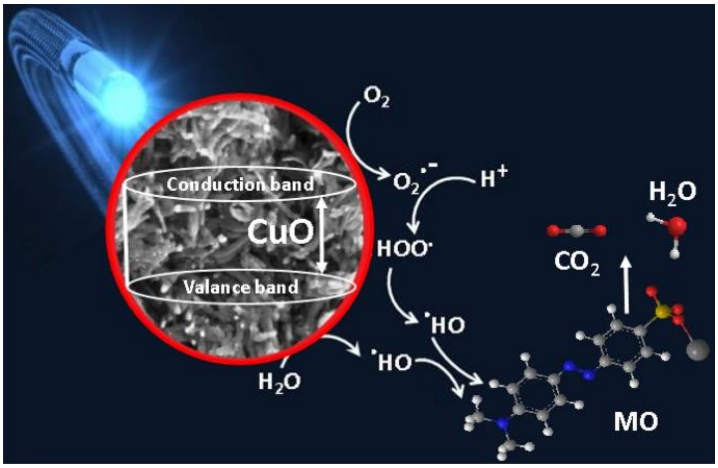

Figure 1: Photocatalytic degradation mechanism of CuO nanocomposite against methyl orange dye [36].

2.4.1. Coupled semiconductors

Coupling of two or more semiconductors with different band gap energies making a heterostructure semiconductor is an effective approach to promote charge separation and minimize or inhibit charge-carrier recombination for improved photocatalytic activity. Many efforts have been made in the synthesis of different coupled semiconductors such as CuO/GO, SnO_2 /TiO_2, ZnO/TiO_2, or CdS/TiO_2 [37]. The synthesized coupled semiconductors significantly enhance the photocatalytic efficiency by decreasing the recombination rate of the photogenerated electron-hole pairs and present potential applications in water splitting, organic decomposition, and photovoltaic devices. These composites were also considered promising materials to develop a high-efficiency photocatalyst activated with visible light. They can also compensate for the disadvantages of the individual components and induce a synergistic effect such as an efficient charge separation and improvement of photostability.

2.4.2. Metal/semiconductor heterostructure nanocomposites

Another effective method for increasing the lifetime of the photogenerated electron-hole pair and hence reducing their recombination is to deposit noble metals on the surface of semiconductors. Earlier investigation revealed that metal/semiconductor composites enhance the efficiency of the photocatalytic process, wherein metal deposits depending upon the work function serve as passive sinks for electrons or holes, hindering the recombination. Due to the different work functions of the metal and semiconductor, a space charge region is created upon their contact and

a built-in potential facilitates the separation and transportation of photogenerated electron-hole pairs similar to that in the coupled semiconductors.

2.5. Metal oxide nanoparticles

Metal oxides are classified as semiconductor materials because of the way that the highly electronegative charges of oxygen atoms combine with those of metallic elements to generate their chemical structures. To maintain their electrical insulator behavior at 0 K, semiconductors must have a structure made up of electronic bands, with the valence band (filled) and conduction band (unfilled) separated by a bandgap that has enough energy (roughly 1.0–3.0 eV) [38]. In addition to their ability to catalyze acid-base reactions, metal oxides in the 1950s attracted interest for their possible involvement in catalytic events (small areas where an acid and a base participate simultaneously) with double acid-base sites [39]. The catalytic surface of metal oxides typically consists of coordinatively unsaturated cationic metal centers, which are Lewis acid sites, and anionic oxygen centers, which are Lewis base sites (O_2^-). Anionic oxygen centers can interact with metals to create ionic bonds because of their high electronegativity. Numerous industrial techniques, including sol-gel, sputter-coating, hydrothermal and precipitation processes, chemical treatments of their precursor reagents, and green synthesis, can be used to create these materials [40]. These synthesis routes enable the production of metal oxides with nanometric-scale particle sizes (of the order of 10^{-9} m), which directly affects the materials' increased surface area/volume ratio and, as a result, their increased application efficiency as functional materials.

When these materials are excited by external environmental stimuli (e.g; light, pressure, electrical field, heat, magnetic field, etc.) with sufficient energy to permit valence band electrons (e-) to migrate to the conduction band, they jump over the bandgap and produce active holes (h+) in the valence band, exhibiting conductor characteristics [38]. The energy structure of their electronic bands, in other words, directly affects their electrical and electronic characteristics.
Given this, metal oxide nanostructures are unique among materials because of their high superficial area/volume ratio and their bulk and surface-derived tunable optical, magnetic, electrical, mechanical, thermal, catalytic, and photochemical properties [41]. These characteristics, along with their outstanding chemical, structural, and environmental stability,

guarantee a wide range of new uses, including the manufacturing of fuel cells, solar cells, electrochemical, optical, and gas sensors, supercapacitors, adsorbents, photocatalysts, and piezoelectric devices [41, 42]. In many chemical reactions, the surface morphology of the majority of metal oxides is crucial. Due to their optical, electronic, magnetic, electrical, and mechanical properties, as well as their high chemical stability and resistance to high temperatures (higher than those seen for polymeric materials), metal oxides have been extensively researched and are therefore appropriate for a variety of scientific and technological applications [42].

2.6. Copper (II) oxide nanoparticles; properties, and its use

Copper is a reddish-brown metal that is used in bulk for more than 20 million tons annually, indicating its great demand. Copper has the electrical configuration [Ar] $3d^{10}$ $4s^{1}$ rather than [Ar]$3d^{9}4s^{2}$ because a fully-filled 3d sub-shell appears to have somewhat lower energy and be slightly more stable [43]. Accordingly, oxygen [He] $2s^{2}$, $2p^{4}$ has an electron configuration of p-block and period 2, while copper is a d-block and period 4 element. CuO (Cupric Oxide) and Cu_2O (Cuprous Oxide) are two significant copper oxide chemicals. Tenorite is the natural form of copper (II) oxide. Pyrolysis of the nitrate, hydroxide, or carbonate salts can produce this black crystalline solid. As for CuO, it is melting and boiling points are 1201 ^{O}C and 2000 ^{O}C, respectively. The mass ratio of the copper (II) oxide complex is 20.10 for oxygen and 79.87 for copper. With a density of 6.31 g/cm^3 and a molar mass of 79.55 g/mol, this inorganic compound has a brown-to-black appearance. In the current days of science and technology, CuO which is also known as cupric oxide has attracted more attention from researchers because of its unique physical and chemical properties such as high electron communication features, low surface area high solar absorbency, and narrow band gap (Eg ~ 1.2 eV).

Being one of the important narrow band gap semiconductors, CuO has shown an excellent performance and thus could be used in a wide range of practical applications. CuO has been explored in different fields of optoelectronics, electronics, biosensors, solar cells, magnetic storage media, optical switches, batteries, and heterogeneous catalysts. For instance, the high theoretical lithium storage capacity lifts CuO as an active anode material for lithium-ion batteries. Other than that, CuO possesses great photoconductive and photochemical properties which make it a potential material for for solar cell fabrication. In addition, it exhibits a higher

surface area relative to its size and morphology thus giving it an advantage as a catalyst in water treatment for removal of dye.

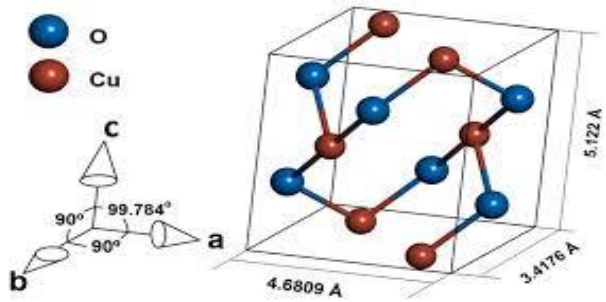

Figure 2: Crystalline structure of copper oxide

2.7. Synthesis approach of nanoparticles

Because of their intriguing size-dependent physical and chemical characteristics as well as their potential for technological use, nanostructured materials have garnered a lot of scholarly interest in their design and fabrication [44]. Such nanoparticles' characteristics are greatly influenced by the synthesis method, and these characteristics in turn greatly influence the applications for which they are used. The techniques used to create nanoparticles may be generally divided into two categories. For instance, the Bottom-up and Top-down processes are shown in Figure 2 below.

i) The top-down strategy (comminution and dispersion) involves using a variety of lithographic processes, including grinding, milling, and others, to break down bulk material into nanoscale particles. Lithography, laser ablation, sputtering deposition, pulsed electrochemical etching, and vapor deposition are some of the most widely used physical processes. Energy can come from mechanical, thermal, or chemical sources. There is a drawback to this approach, too, in that it will produce particles with a broad size distribution. ii) Bottom-up (approach nucleation and growth): Beginning with a simple metal salt, the bottom-up method gradually transforms it from ions to elemental atoms through chemical means before clumping and growing into nano-size particles. It is thought to be easier and more advantageous when creating nanoparticles smaller than 100 nm. Typically, the "bottom-up" approach uses a variety of processes, including sol-gel, solvothermal decomposition, pyrolysis, photochemical reduction, microemulsion, and microwave assistance, to create NPs from atoms or molecules [45].

2.8. Clay structure and utilization in catalysis

Clays are silica-alumina minerals that have layered structures made of aluminum silicates that are arranged in tetrahedral and octahedral sheets. The layers have net negative charges and include cations that fill the inter-lamellar region, such as Na^{+}, K^{+}, Ca^{2+}, and so on. Clays are amenable to alteration because of the cations' exchangeable characteristics, which make it simple to swap them out for different cations or molecules. The layered structure and the ion exchange process control whether metal cations and molecules may be covalently bonded to layer atoms. The following classes of clay minerals are distinguished: kaolinite, smectite, vermiculite, illite, and chlorite [46]. The most common clay class for supporting metal and metal oxide catalysts is smectite, which is used for both advanced oxidation processes and some catalyzed organic reactions. Smectite, sometimes referred to as a 2:1 layer or T-O-T clay mineral, is a member of the hydroxyl alumino-silicates group and is made up of two layers of tetrahedral silica and one layer of octahedral alumina group [47]. Natural weathering of soils or volcanic ash produces smectites, which include montmorillonite, saponite beidellite, nantronite, and hectorite. The chemical composition of the smectite group of clays varies, with Fe^{2+}, Mg^{2+}, or Mn^{2+} replacing Al^{3+} in the octahedral cation sites and Al^{3+} or Fe^{3+} replacing Si^{4+} in the tetrahedral cation sites [48]. Because smectite structures are easily hydrated and have a high cation exchange capacity, they enhance swelling capacities. Their large surface area, which is a result of their thin layers and tiny particle sizes, allows them to absorb a wide range of materials, including organic molecules. Vermiculite, also known as T-O-T clay or 2:1, has a similar structure. Because vermiculite isomorphously substitutes lower-valence ions for higher-valence ions in both the octahedral and tetrahedral sheets (for example, Al^{3+} for Si^{4+} and Mg^{2+} or Fe^{2+} for Al^{3+}), it has more negatively charged plate surfaces than smectite [49, 50]. In contrast to vermiculite and smectite, kaolinite is a 1:1-type clay mineral made up of one layer of octahedral alumina group (TO) and one layer of tetrahedral silica. $Al_2O_3 \cdot 2SiO_2 \cdot 2H_2O$ is the chemical formula for several minerals, such as kaolinite, nacrite, dickite, and halloysite (39% Al_2O_3, 46.5% SiO_2, and 14.0% H_2O) [49].

2.9. Clay modifications

2.9.1. Impregnation

The dispersion of metal and metal oxide nanoparticles into non-swelling clays, such as kaolinite, halloysite, dickite, and nacrite, is usually conducted by the impregnation method, even though the procedure can also be conducted for swelling clay. The impregnation mechanism depends on the metal precursor and can be assisted by severe intensification procedures such as hydrothermal, microwave, and ultrasound irradiation. Various techniques, such as the sol-gel method, co-precipitation, wet impregnation, and their combinations, have been performed and chosen based on the technical characteristics of the metal precursor. Sol-gel dispersion is usually performed because metal oxide formation can be achieved through polymerization in sol-gel systems. Pillarization by using organo-metal precursors, such as metal alkoxides (such as titanium isopropoxide, titanium isobutanate, and zirconium isopropoxide), and acetate salts, usually occur within this mechanism. Wet impregnation and co-precipitation are based on the homogeneously dispersed metal salt in the clay suspension, in which the co-precipitation conducted by the additive base environment forms the deposited metal hydroxide. The dispersion of TiO_2 in kaolinite and hectorite using titanium isopropoxide can be conducted by a sol-gel mechanism due to Ti-O-bond formation via polymerization [49].

Using different precursors, such as $TiOCl_2$ and $TiOSO_4$, the impregnation can be conducted by depositing titanium salt into clay suspension or through the co-precipitation method. Temperature, pH, and the precursor solvent are crucial factors in determining the particle size and distribution of the metal oxide in clay supports. Research on TiO_2/kaolinite using titanium isopropoxide demonstrated the role of the DMSO solvent in producing more space for the more homogeneous dispersion of TiO_2, which furthermore determines the hydrophobicity and reactivity of the nanocomposite [51]. The impregnation method including wet impregnation consists of mixing a precursor salt with a clay suspension in a solvent and tuning the optimum pH. As an example, the impregnation of TiO_2 into kaolinite utilizing $TiOSO_4$ was optimally conducted in an acidic mixture to maintain the ionic form of Ti^{4+} in the solution [52]. The co-precipitation method was reported in the synthesis of ZnO/montmorillonite. The combination of the sol-gel mechanism and wet impregnation method can also be conducted. In a different scheme, the composite formation of MnO_2 nanosheets and MnO_2 nano-wire with montmorillonite was achieved under hydrothermal conditions. For both inserted MnO_2

nanostructures, $KMnO_4$ solution was employed as a precursor, and a hydrothermal procedure was conducted in a Teflon-lined stainless-steel autoclave. MnO_2 nanosheets were formed at 160°C for 24 h over the mixture of the precursor solution and montmorillonite suspension. Meanwhile, for the MnO_2 nanowire, a combination of $KMnO_4$ and $(NH_4)_2S_2O_8$ under hydrothermal treatment at 90°C for 12 h was performed.

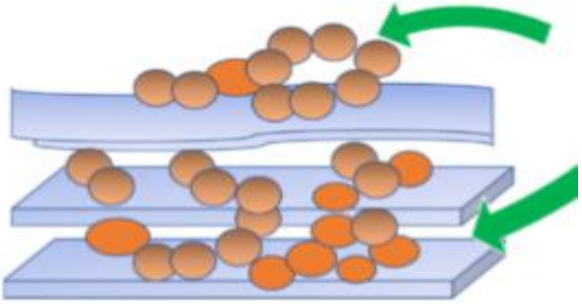

Figure 3: The possible formation of porous structures and new surfaces as adsorption sites by metal/metal oxide impregnation.

2.9.2. Pillarization

Pillarization is a popular mechanism of clay modification by metal oxide insertion to swelling cla ys such as smectite and vermiculite. The process consists of intercalation followed by a calcinati on procedure. Intercalation is an ion exchange process of native cations between the smectite lay ers with other cations having a higher reduction potential, or the polyoxocations [53]. The interca lation is intended to open up the interlayer region, creating a higher specific surface area or pore volume; furthermore, through the calcination process, dihydroxylation of the polyoxocations will produce a metal oxide as metal oxide pillars which is also homogeneously distributed metal oxid e. The stability of polyoxocations is the main factor for pillarization; therefore, the optimum con ditions for some metal oxide pillaring precursors were studied. The polyoxocation of the Keggin ion Al is reported to be the best pillaring precursor for Al_2O_3, which can be prepared by the slow titration of Al salt with -OH at an Al: OH molar ratio of 1:1.

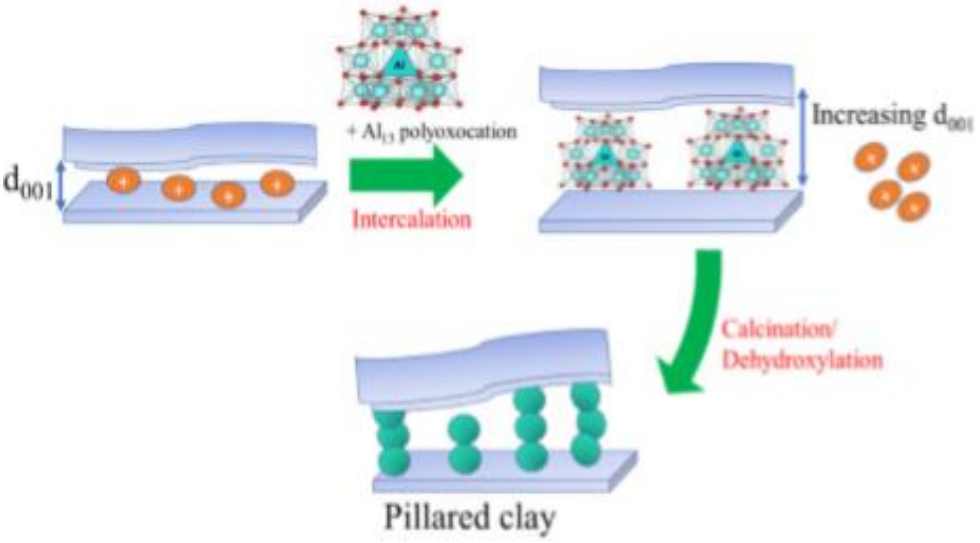

Figure 4: Schematic representation of clay pillarization.

2.10. Wastewater treatments

Water is one of the natural resources that billions of people depend on to survive, and it has a big impact on world agriculture, ecosystems, and health. Dyes are organic and hence are rendered as impurities. They produce perilous by-products in wastewater via oxidation, hydrolysis, and other chemical reactions [54]. The question arises: at what concentration do these dyes pose a risk to life and aquatic life? The textile industries significantly contribute to aqua pollution. They cause skin sensitization, respiratory and heart problems, and irritation; therefore, their disposed water must be treated per health standards [55]. Complete mineralization of the organic components takes place without leaving any harmful by-product at all. These methods include biological, chemical, physical, and AOPs [56]. Reducing contamination in industrial discharge and improving the use of treated water in sectors like the petrochemical and building industries are two main drivers for water treatment. Cost-effectiveness is another factor affecting the treatment method choice.

2.10.1. Conventional wastewater treatment technology and its drawbacks

2.10.1.1. Biological methods

Implementing biological methods has garnered recognition as viable and profitable solutions and environmentally friendly alternatives to conventional industrial wastewater treatment practices.

These innovative processes use diverse natural agents, including microorganisms, bacteria, fungi, yeasts, algae, and enzymes, to facilitate biodegradation. Using these microbial and enzymatic activities, aerobic, anaerobic, or combined processes, ensures the efficient breakdown and elimination of pollutants in the wastewater, ultimately promoting a healthier and more sustainable ecosystem. Biological methods have multiple requirements, and many factors act as limiting factors in this scenario. For instance, daytime variation, the toxicity level of pollutants, acidity, alkalinity, etc., many organic dyes are efficiently reduced by this method. Still, at the same time, others are highly unmanageable owing to their structure and synthetic origin. The chemical method employs several chemicals in the same flow, and the produced sludge further requires treatment. Due to these factors, it is a costly process.

2.10.1.2. Physical methods

The physical methods include membrane-based filtration processes and adsorption processes. The problem usually encountered in membrane-dependent operations is the lifetime of the membrane. These cliché methods, although in industrial usage, are still ineffective in either completely removing the effluents from the water discharge or failing in removing the substances that are not readily absorbed to be removed.

2.10.1.3. Chemical methods

The chemical activities of OH are robust oxidation processes that remove hazardous organic molecules from the water. Every chemical purification technique used today uses dangerously strong oxidants or highly energetic ultraviolet radiation. Specific chemical refinement techniques, such as direct photolysis and the use of strong oxidants like H_2O_2/O_3/UV, H_2O_2/UV, and O_3/UV, can have a direct negative impact on the environment. Nonetheless, identifying running method parameters depends on the type of contamination present. Contemporarily, a relatively new technique is known as advanced oxidation. The process is promising because it reduces the organic components to CO_2 and H_2O.

2.11. Dyes

Potable water is increasingly becoming scarcer due to increased contamination of surface and ground water. The main causes of surface and groundwater contamination are industrial effluents (even in small amounts), excessive use of pesticides, fertilizers (agrochemicals), and domestic waste landfills. Organic pollutants such as dyes (malachite green, methylene blue, methyl orange, Congo red, etc.,) that are non-biodegradable and highly toxic pose a great threat to aquatic life and other living organisms [54]. Many of the organic dyes along with their products have a carcinogenic effect on human beings. Consequently, it is a matter of great concern to treat these dyes before discharging them. Among these organic dyes malachite green (MG), has been extensively used in the textiles and printing industry which has some serious harmful effects on humans and animals [56]. Malachite green dye is a heterocyclic aromatic chemical compound (shown in Figure 5 below) with the molecular formula $C_{23}H_{25}ClN_2$ having a molar mass of 364.911g/mole and λmax of 618nm. The chemical name according to the International Union of Pure and Applied Chemistry (IUPAC) is 4-{[4-(Dimethylamino)phenyl](pheny)methyliene}-N, N-Dmethylcyclohexa-2,5-dien-1-iminium chloride. If MG is ingested stimulates the gastrointestinal tract and leads to nausea, vomiting, and diarrhea. Because of the potential toxicity of MG on humans, animals, and aquatic life and its visibility in surface waters, degradation of it has been a matter of considerable interest.

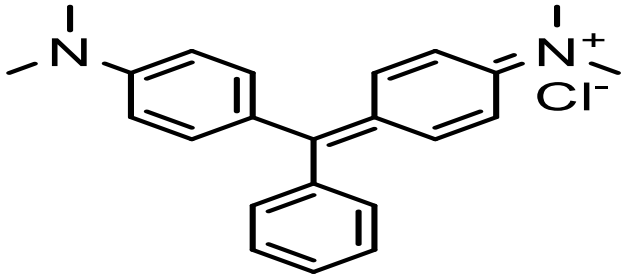

Figure 5: Structure of MG Dye

2.12. Photocatalysis

AOPs are promising techniques for wastewater treatment as they convert toxic organic substances into nontoxic components, i.e., water and carbon dioxide [57]. The term photocatalysis is formed by combining two words, photo and catalysis. A catalyst is a reagent that causes the chemical reaction to speed up by usually lowering the activation energy for the substrate. The photocatalyst is a substance that does the same but with the help of sunlight. The best example in this regard is photosynthetic machinery. In the process, chlorophyll acts as the

photocatalyst. Both photosynthesis and photocatalysis are analogous in function since both work as light-harvesting systems; chlorophyll absorbs the sunlight and converts water and carbon dioxide to glucose and oxygen. Similarly, photocatalysis yields strong oxidizing agents, transforming the organic matter into water and carbon dioxide in the presence of sunlight, water, and a catalyst.

2.12.1 Advanced oxidation processes (AOPs)

It has been frequently observed that pollutants not amenable to biological treatments may also be characterized by high chemical stability and/or by strong difficulty in being completely mineralized. In these cases, it is necessary to adopt reactive systems much more effective than those adopted in conventional purification processes. As a response, the development of newer eco-friendly methods of destroying these pollutants became an imperative task. Thus, over the past decade, many research efforts have been devoted around the world to developing a newer, more powerful, and very promising technique called AOPs to treat the contaminants of drinking water and industrial effluents. AOPs are defined as "near ambient temperature and pressure water treatment processes which involve the generation of hydroxyl radicals in sufficient quantity to effect water purification" [58]. Although it is claimed that there are other species involved, the active species responsible for the destruction of contaminants in most cases seems to be the hydroxyl radical ($OH^{\bullet}$) which is unstable and quite reactive. Due to the instability of $OH^{\bullet}$ radical, it must be generated continuously "in situ" through chemical or photochemical reactions [59]. The hydroxyl radical ($OH^{\bullet}$) is a powerful, non-selective chemical oxidant, which acts very rapidly with most organic compounds. After fluorine, the hydroxyl radical is the second strongest known oxidant having an oxidation potential of 2.8 V [60]. It can able to oxidize and mineralize almost every organic molecule yielding H_2O, CO_2, and inorganic ions. One of the mechanisms for the oxidation of organic molecules by hydroxyl radical is the abstraction of hydrogen from organic molecules (Eq. 2.1) [60]. This reaction generates organic radicals which by the addition of molecular oxygen yield peroxyl radicals (Eq. 2.2). These intermediates initiate thermal (chain) reactions of oxidative degradation, leading finally to carbon dioxide, water, and inorganic salts. Besides hydrogen abstraction, electron transfer to hydroxyl radicals (Eq. 2.3) constitutes another mechanism of oxidative degradation. Reaction (2.3) combined with a subsequent proton transfer can hardly be differentiated from Eq. 2.1.

$$\dot{OH} + R \rightarrow HO_2 + \dot{RH} \quad (2.1)$$

$$\dot{R} + O_2 \rightarrow \dot{R}O_2 \rightarrow \text{Products} \quad (2.2)$$

$$H\dot{O} + RH \rightarrow H\dot{O} + R\dot{X} \quad (2.3)$$

The reaction scheme demonstrates that the rate and efficiency of oxidative degradation processes, which are primarily based on the production and the reactivity of radical intermediates, depend on the energy needed to homolyze a given chemical bond, and to a large extent on the concentration of dissolved molecular oxygen [60].

2.12.2. Heterogeneous photocatalysis

The process is heterogeneous because there are two active phases, solid and liquid. Photocatalysis differs from other AOPs because it employs low-energy UV light and reusable catalysts, and it does not require the addition of any other strong oxidants. This process can also be carried out utilizing the near part of the solar spectrum (wavelength shorter than 380 nm) which transforms it into a good option to be used on a big scale. One of the major applications of heterogeneous catalysis is photocatalytic oxidation to achieve partial or total mineralization of gas phase or liquid phase contaminants to benign substances. The oxidizing species generated in the photocatalytic process are either bound hydroxyl radicals or free holes. Even though degradation begins with a partial degradation, the term photocatalytic degradation usually refers to complete photocatalytic oxidation or photo mineralization, essentially to CO_2, H_2O, NO_3^-, PO_4^{3-} and halide ions [60]. The advantages of heterogeneous photocatalysis process over other conventional methods can be summarized as follows: (i) the processes can be carried out under ambient condition (temperature and pressure); (ii) the process uses atmospheric oxygen as oxidant and no other expensive oxidizing chemical is required; (iii) the oxidant is strong and less selective which leads to complete mineralization of almost all organic pollutants in wastewater; (iv) this process is known as green technology because degradation products (carbon dioxide, water and mineral acids) show moderate toxicity; (v) no residue of the original material remains and therefore no sludge requiring disposal to landfill is produced in this process; (vi) in addition, this process can be carried out at extremely low concentrations because the pollutants is strongly adsorbed on the surface of the catalyst, allowing sub part-per-million condition; (vii) the photocatalysts are cheap, non-hazardous, stable, biologically and chemically inert, insoluble under most conditions and reusable. Summing up all these benefits and advantages,

heterogeneous photocatalysis provides a cheap and effective alternative to clean water production and environmental remediation.

2.12.3. Basic principle of photocatalysis

In the photocatalytic oxidation process, organic pollutants are destroyed in the presence of semiconductor photocatalysts (e.g. TiO_2, ZnO), an energetic light source, and an oxidizing agent such as oxygen or air. The first step in the heterogeneous photocatalysis of organic and inorganic compounds is the interaction of semiconductors with light which results in the generation of electron-hole pairs in the semiconductor particles. When a semiconducting photocatalyst is illuminated with light the energy of which is equal to or greater than the band-gap energy, light is absorbed by the semiconductor and the valence band electrons are excited to the conduction band, leaving a positive hole in the valence band as indicated in Figure 6 below [60].

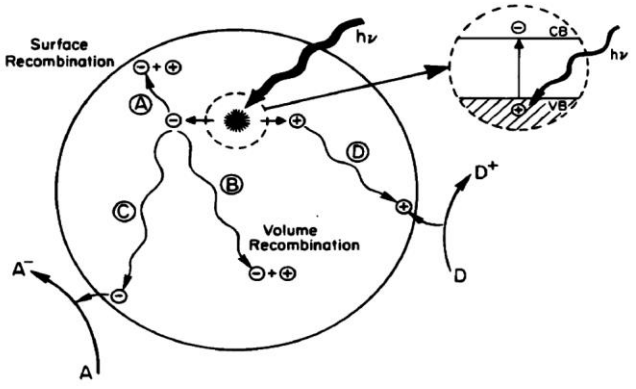

Figure 6: Photoexcitation in a semiconductor photocatalyst

The excited state conduction-band electrons and valence-band holes can then follow several pathways. The photoinduced electrons transfer to adsorbed organic or inorganic species or the solvent results from the migration of electrons and holes to the semiconductor surface. The electron transfer process is more efficient if the species are pre-adsorbed on the surface [61]. While at the surface the semiconductor can donate electrons to reduce an electron acceptor (usually oxygen in an aerated solution) (pathway C), a hole can migrate to the surface where an electron from a donor species can combine with the surface hole oxidizing the donor species (pathway D). The probability and rate of the charge transfer processes for electrons and holes

depend on the respective positions of the band edges for the conduction and valence bands and the redox potential levels of the adsorbed species.

In competition with charge transfer to adsorbed species are electron and hole recombination. Recombination of the separated electron and hole can occur in the volume of the semiconductor particle (pathway B) or at the surface (pathway A) with the simultaneous release of heat. Oxygen is the usual electron acceptor employed in studies aimed at using semiconductor photocatalysis for environmental cleaning; its role in these reactions has been the focus of attention in several theoretical and experimental studies [62]. It is generally admitted that photogenerated electrons can reduce molecular oxygen to $O_2^{\bullet}$ which can be subsequently transformed into other chemical species, such as HO_2 HO_2–, H_2O_2, and possibly HO• radicals [61]. On the other hand, photogenerated holes can oxidize the electron donor (also referred to as the "hole scavenger"), either via the formation of reactive species such as surface-bound $HO^{\bullet}$ radicals or through direct reaction with adsorbed organic molecules [63]. These reactions can ultimately result in the complete photomineralization of the organic compounds to carbon dioxide, water, and mineral acids.

2.12.4. Mechanism of generating oxidizing species

Heterogeneous photocatalysis is a complex sequence of reactions. In the classical heterogeneous photocatalytic process, the reaction itself occurs in the adsorbed phase and the overall process can be decomposed into five independent steps: [64]. (i) mass transfer of the reactants in the liquid phase to the surface of the catalyst; (ii) adsorption of the reactants onto the photon-activated catalyst surface (i.e. surface activation by photon energy occurs simultaneously in this step); (iii) photocatalysis reaction for the adsorbed phase on the catalyst surface; (iv) desorption of the products from the catalyst surface; (v) desorption of the products from the surface of the catalysts. There are two pathways through which OH radicals can be formed. The valence band hole (h^+_{VB}) can either react with the adsorbed water or the adsorbed hydroxyl groups (OH^-) on the semiconductor photocatalysts (SC) as shown by Eq. (5) and Eq. (6).

$$SC + hv \rightarrow SC(e^- CB + h^+ VB) \quad (2.4)$$

$$SC\,(h^+ VB) + H_2O(ads) \rightarrow SC + \dot{H}O + H^+ \quad (2.5)$$

$$SC(h^+ VB) + HO^- \rightarrow SC + \dot{H}O + (ads) \quad (2.6)$$

To oxidize hydroxide ions or water, the oxidation potential for reactions (5) and (6) must lie above (i.e., be more negative than) the upper energy level position of the semiconductor valence band. It is generally accepted that oxygen plays an important role in photocatalysis. Oxygen can trap conduction band electrons to form superoxide ion $O_2^{\bullet -}$ as shown in Eq. (7). These superoxide ions can react with hydrogen ions (formed by water splitting), forming $HO_2^{\bullet}$.

$$SC\,(e^{-}VB) + O_2\,(ads) \rightarrow SC + O_2^{\cdot -}(ads) \quad (2.7)$$

$$O_2^{\cdot -} + H^{+} \rightarrow HO_2^{\cdot} \quad (2.8)$$

H_2O_2 could also be formed from $HO_2^{\bullet}$ species according to the following reaction

$$SC\,(e^{-}VB) + O_2^{\cdot -} + H^{+} \rightarrow SC + H_2O_2 \quad (2.9)$$

The photogenerated hydrogen peroxide undergoes further decomposition to yield hydroxyl radicals.

$$H_2O_2 + hv \rightarrow 2HO \quad (2.10)$$

$$H_2O_2 + O_2^{\cdot -} \rightarrow HO + O_2 + \dot{O}H \quad (2.11)$$

$$H_2O_2 + SC(e^{-}VB) \rightarrow \dot{H}O + OH^{-} + SC \quad (2.12)$$

It should be mentioned that it takes three electrons to produce one hydroxyl radical through the above pathway, but it takes only one hole to produce a hydroxyl radical from adsorbed water or hydroxyl group. Therefore, most of the hydroxyl radicals are generated through hole reactions. Nonetheless, the presence of electron scavengers (adsorbed oxygen) is vital for prolonging the recombination and successful functioning of the photocatalysis process. Eq. (7) depicts how the presence of oxygen prevents the recombination of electron-hole pairs while allowing the formation of superoxide radicals. On the other hand, without the presence of water molecules, the highly reactive hydroxyl radicals could not be formed and impede the photodegradation of liquid phase organics. This was evidenced by a few reports that the photocatalytic reaction cannot proceed in the absence of water molecules [65]. The hydroxyl radical generated from the oxidation of adsorbed water where it is adsorbed as OH^{-} is the primary oxidant for the degradation of organic pollutants. Oxidation of organic compounds proceeds through several free radical reactions, producing a large number of intermediates, which in turn, undergo oxidative cleavage, ultimately resulting in the formation of carbon dioxide, water, and inorganic ions. In the photocatalytic degradation of pollutants, when the reduction process of oxygen and the oxidation of pollutants do not advance simultaneously, there is an electron accumulation in the CB, thereby causing an increase in the rate of recombination of e^{-}_{CB} and h^{+}_{VB} [66].

2.13. Characterization

2.13.1. Powder x-ray diffraction (XRD)

X-ray diffraction is a versatile, non-destructive analytical method for the identification and quantitative determination of various crystalline forms, known as 'phases' of compounds present in powder and solid samples [67]. Diffraction occurs as waves interact with a regular structure whose repeat distance is about the same as the wavelength. It happens that Xrays have wavelengths of the order of a few angstroms, the same as typical inter-atomic distances in crystalline solids. That means X-rays can be diffracted from minerals which, by definition, are crystalline and have regularly repeating atomic structures. When certain geometric requirements are met, X-rays scattered from a crystalline solid can constructively interfere, producing a diffracted beam. XRD is a non-destructive analytical technique that can be applied for the identification of unknown specimens and the determination of material properties. It is the most important and beneficial technique in solid-state chemistry and it has been applied for the fingerprint characterization of crystals and the determination of their structures.

2.13.2. Scanning electron microscopy (SEM)

The image from SEM gives a clear picture of the morphology of the as-synthesized product, the surface morphologies and particle size distribution of the photocatalyst were characterized by SEM. It is an electron microscope that provides information about a sample's surface topography, composition, and other surface properties such as electrical conductivity. In SEM, it is possible to observe and characterize the heterogeneous organic and inorganic materials on a nanometer (nm) to micrometer (μm) scale.

2.13.3. UV-Visible spectroscopy (UV-Vis)

Optical absorption plays an important role in photocatalysis, especially in the visible light photo-degradation of contaminants [68]. Based on the diffuse absorbance spectra of the materials, the absorption edge wavelength and band gap energies of the as-synthesized samples were determined and compared. The wavelength at the absorption edge for a semiconductor is determined as the intercept on the wavelength axis for a tangential line drawn on the absorption spectrum. Diffuse reflectance spectroscopy is a sensitive technique that uses the interaction of

light, absorption, and scattering to produce a characteristic spectrum providing information regarding the structure and composition of the material. Electronic transition in materials can be observed in a liquid state using UV-visible spectroscopy. But in the case of insoluble solids, UV-visible diffuse reflectance is used as a solid. It is used to study the electronic transitions between orbitals or bands in the case of atoms, ions, and molecules in gas, liquid, or solid state. This technique is performed based on electronic excitation by the absorption of light.

2.13.4. Fourier transform infrared spectroscopy (FTIR)

FTIR is used to determine the presence of functional groups by measuring the vibrational frequencies of chemical bonds. Although it is non-destructive, the approach has a high signal-to-noise ratio, making it challenging to analyze samples with weak spectra and low transmission. By using metal oxide nanoparticles and infrared (IR) observing the stretching mode's presence or absence associated with complexes present in fully oxidized nanoparticles, the oxidation state and surface structure of metal-oxide nanoparticles are demonstrated.

CHAPTER THREE

3. MATERIAL AND METHODS

3.1. Sample site

The sample of clay soil was collected in the Amhara region in the north part of Ethiopia from the Awi zone in Dangla word at Ligaba kebele environment; the sample was taken from 3.5 m under the surface horizon of the earth. The sample location was found near Abay River (Blue Nile) 20 km in the west relative to Dangla town, 68 km far from Bahir Dar in North West, and 500 km to Addis Ababa in North West. The soil was collected using a hand drill and taken into BDU laboratory class in a plastic bag and it was preserved in a polyethylene bag.

3.2. Apparatuses and instruments

The materials and apparatus used were: FTIR, UV-Vis, XRD, SEM-EDX, analytical balance, pH Meter, agate mortal, thermometer, furnace, crucible, hot plate, centrifuge, volumetric flask, pipettes, magnetic stirrer, auto incubator test tubes, ultrasonic, beakers, etc.

3.3. Chemicals and reagents

The chemicals used included: copper (II) sulfate penta hydrated [$Cu(SO_4)•5H_2O$, 98%], clay, ethanol (C_2H_5OH), malachite green dye [$C_{23}H_{25}ClN_2$, 96%], de-ionized water, hydrochloric acid (HCl, 37%), and sodium hydroxide (NaOH, 98%) were purchased from Sigma Aldrich. All other chemicals are of analytical reagent grade and were used directly without further purification. During the experiment, distilled water was used for the preparation of all solutions.

3.4. Synthesis of copper oxide nanoparticles (CuO NPs)

The co-precipitation method was used to synthesize CuO NPs from $Cu(SO_4)•5H_2O$, and NaOH (0.2 M aqueous solution) in ethanol. For CuO NPs preparation, 4.994 g of $Cu(SO_4)•5H_2O$ was added to a 250 mL Erlenmeyer flask containing 100 ml of ethanol and heated to 70 °C while continuously stirring. 0.2 M NaOH solution was added to the stirred solution dropwise until a pH of 12 was reached and until the color change was observed from green to black. The formation of a black color confirmed $Cu(OH)_2$ amorphous [69]. The filtered dark residual sample was washed with deionized water to remove sulfate ions multiple times and centrifuged at 4000 rpm for 15

minutes. The product was dried in an oven at 70 °C for 12 hr and then calcinated at 450 °C for 4 hr. obtained CuO NPs.

$$CuSO_4.5H_2O + 2NaOH \rightarrow Na_2SO_4 + Cu(OH)_2 \quad (3.1)$$

$$Cu(OH)_2 + Heat \rightarrow CuO + H_2O \uparrow \quad (3.2)$$

3.5. Synthesis of clay-supported CuO nanocomposites

The dispersion of metal oxide nanoparticles into the natural clay structure can be conducted by an ion exchange process of the metal ions with native cations of the clay mineral and the in-situ dispersion of metal oxide nanoparticles into the natural clay structure. Clay-supported CuO NCPs were prepared with slightly modified procedures [70, 71]: the dried sample (natural clay) was ground into powder or pieces using a mortar and pestle. 10 grams of grounded powdered clay sample were dissolved in 1000 ml of distilled water and shaken using an electronic shaker at 150 rpm for 72 hr at room temperature. The solution was decanted and washed several times using distilled water to remove impurities. The wet clay sample was dried in the oven at 100 °C for 12 hr followed by sieving through a 250 µm sieve to ensure the required sample homogeneity (uniform texture) and stored in tight polyethylene bags labeled as clay sample A and stored in cooled and dry place until further use. 30 ml of clay solution prepared from sample A was added into a solution containing 0.2 M $CuSO_4.5H_2O$ (4.994 g) with adjusting by NaOH, drop by drop under vigorous magnetic stirring over copper sulfate solution at a pH of 10.7. Then the reaction mixture was heated at 70 °C for 24 hr and the cooled dark brown residual sample was washed with deionized water to remove sulfate ions multiple times and centrifuged at 4000 rpm for 15 minutes. The product was dried in an oven at 80 °C for 12 hr and then calcinated at 450 °C for 4 hr. The obtained product is called clay-supported CuO NCPs.

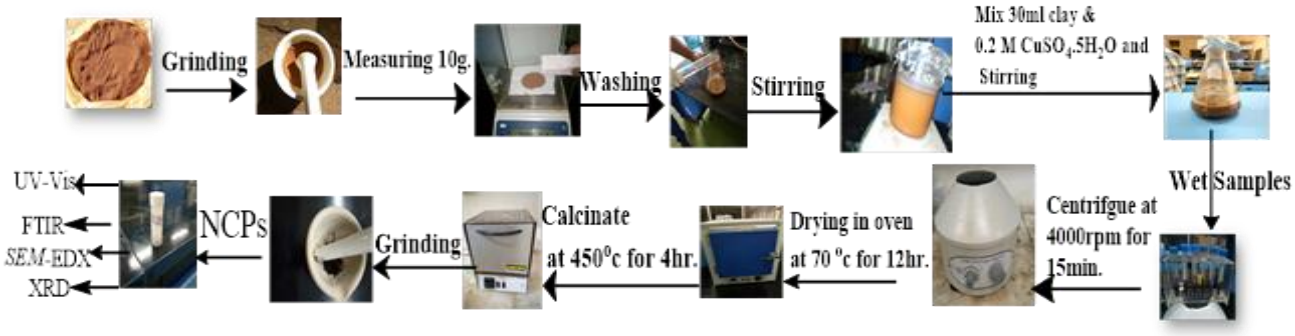

Figure 7: Synthesis path of clay-supported CuO NCPs.

3.6. Preparation of aqueous solution of malachite green (MG)

A stock solution of MG containing 0.5 percent was used. To make the required aqueous solution of MG a stock solution with distilled water was dissolved in a volumetric flask with varied amounts of volume.

3.7. Characterization of nanoparticles (NPs) and nanocomposites (NCPs)

The synthesized CuO NPs and clay-supported CuO NCPs were characterized using Fourier Transform Infrared Spectroscopy (FTIR), Ultraviolet-Visible (UV-Vis) Spectroscopy, X-ray Diffraction (XRD), and Scanning Electron Microscope along with Energy-dispersive X-ray analysis (SEM-EDX).

3.7.1. X-ray diffraction (XRD) analysis

The XRD technique was used in this study the crystalline phase to identify and confirm the structure of CuO NPs and clay-supported CuO NCPs. XRD patterns of the as-synthesized photocatalysts were obtained using a BRUKER D8 Advance XRD, AXS GMBH, Karlsruhe, West Germany X-ray diffractometer (XRD) equipped with a Cu target for generating a Cu Kα radiation (wavelength 1.5406 Å). The measurements were made at room temperature and the accelerating voltage and the applied current were 40 kV and 30 mA, respectively. The instrument was operated under step scan type with step time and degree (2θ) of 1 s and 0.020°, respectively, for 2θ range of 4° to 64°. The identification of a species from its powder diffraction pattern is based on the position of the lines (in terms of 2θ) and their relative intensities. The identification of CuO NPs and clay-supported CuO NCPs crystalline characteristics and crystalline size were characterized by XRD using Shimadzu XRD 6000 Diffractometer with Cu Kα radiation (Voltage = 40 kV, Current = 30 mA, λ = 1.5406 A^o, scan rate of 2.0 min^{-1} and scan range of 2θ from 10-80^o). From the XRD data obtained [72], the crystalline size of synthesized CuO NPs and clay-supported CuO NCPs was obtained from the Debye-Scherrer's Equation as shown below:

$$\mathbf{D} = \frac{\boldsymbol{\kappa\lambda}}{\boldsymbol{\beta\cos\theta}} \qquad (3.3)$$

Where,

k = Scherrer constant (usually 0.9)

λ = Wavelength of the X-Ray source, Cu Kα radiation (1.5406A^o)

β = Full width at half-maximum (FWHM) of the diffraction peak in radian

θ = Bragg's diffraction angle.

β obtained from the XRD data was converted to radian unit using the equation shown below:

$\boldsymbol{\beta}$ = FWHM in $2\theta \frac{\boldsymbol{\pi}}{\mathbf{180}}$

3.7.2. Absorption edge determination

For the estimation of the absorption edge of the as-synthesized photocatalysts, UV–Vis diffuse absorption was measured using an SP65 spectrophotometer at Bahir Dar University research laboratories, scanning over 200-800 nm. About 1 mg nanocomposite was taken in 10 mL of DW, and sonication was performed by a Sonar-made (40 kHz) ultrasonicator.

3.7.3. Fourier transforms infrared spectroscopy

FTIR spectra of the synthesized sample of CuO NPs and clay-supported CuO NCPs were recorded and compared using FT/IR-6600 FT-IR spectrometer (JASCO International Co., Ltd., Tokyo, Japan) Spectrometer using KBr pellet method scanning from 4000 cm^{-1} to 400 cm^{-1}. CuO NPs and clay-supported CuO NCPs were crushed and sieved through a 125μm pore size sieve before being subjected to FTIR analysis [73].

3.7.4. Scanning electron microscopy

SEM is a powerful imaging technique that uses a focused beam of electrons to scan the surface of a sample. It produces high-resolution images, allowing for detailed observation of the sample's morphology, structure, and composition at the nanoscale (1 to 100 nanometers) and microscale (1 micrometer and above). It provides high-resolution images of nanostructures, allowing researchers to analyze their morphology, size, and distribution.

3.8. Photocatalytic degradation studies

Catalytic activities of the as-synthesized photocatalysts were studied for the degradation of MG. The experiment was carried out under visible light illumination (254 nm) using as-synthesized photocatalysts. 0.0164g of the as-synthesized photocatalyst powder and 50 ml of aqueous solution of MG (20 ppm) were taken in a cardboard box and the suspension was stirred in the dark for 30 minutes to obtain adsorption/desorption equilibrium before irradiating the dye in the

reactor [74]. A tungsten lamp (TORCH) with definite power 200W, 220 V, 0.18 A, and 50 Hz frequency was employed as a visible source and positioned parallel to the reactor. The distance between the top of the reactor and the lamp was 9 cm. 10 ml of the sample was withdrawn at 30-minute intervals. The suspension was centrifuged at 3000 rpm for 5 minutes and filtered to remove the catalyst particles before measuring the absorbance. The absorbance of MG solution was determined at a wavelength of 617 nm at pH 7, and light intensity at 8.26 mW/cm^{-2}, and the percentage degradation of MG was calculated using equation 3.4 written below [75]:

$$\text{Removal Percentage \%} = \frac{Co - Ct}{Co} x100 \qquad (3.4)$$

Where C_0 is the initial concentration of the dye, and C_t is the concentration of the dye at time t. Since the concentration is directly proportional to the absorbance (A), the percentage of degradation can be easily calculated using the UV−Vis spectrum. The decrease in absorbance of samples at λmax (617 nm for MG) at various time intervals indicates the rate of decolorization and in turn the degradation efficiency of metal NPs. Furthermore, the rate of the dye degradation was measured at a given time (t) using equation 3.5 written below. The catalytic reaction follows pseudo-first-order kinetics, and the rate constant of the reaction (k) was calculated using $\ln(C_t/C_o)$ vs time plot [76].

$$ln \frac{Ct}{Co} = -\kappa t \qquad (3.5)$$

CHAPTER FOUR

4.1. Characterization

4.1.1. UV-Vis analysis

Figure 8 shows the UV-Vis absorption spectra of clay (a), CuO (b), and clay-supported CuO NCPs (c) examined at 264, 222, and 226 nm, respectively. However, a blue shift was observed in composite 'c' compared to 'a'. This may be due to the synergetic effect of the excess concentration of CuO presence in clay-supported CuO NCPs (Tables 4 and 5).

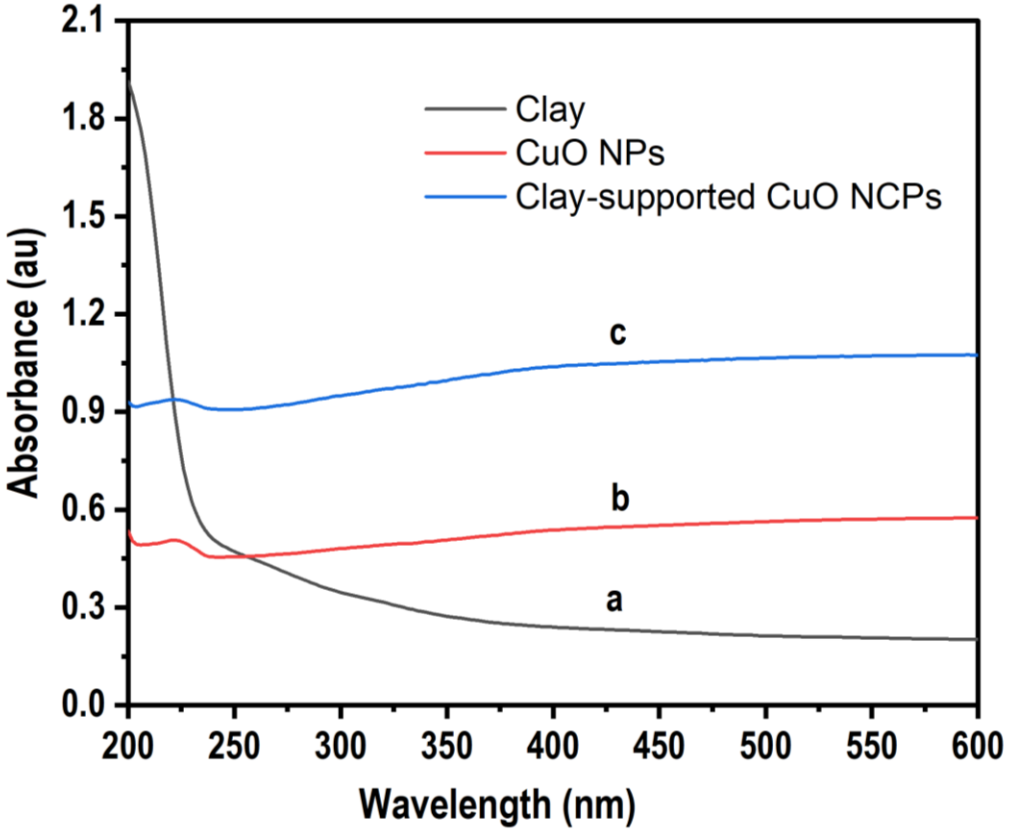

Figure 8: UV-Vis absorption spectra of clay (a), CuO (b), and clay-supported CuO NCPs (c).

4.1. 2. FTIR analysis

FTIR measurement shown in Figure 9 is carried out by scanning 400-4000 cm^{-1} for CuO and clay-supported CuO NCPs with characteristic peaks ranging from 516cm^{-1} to 3454$cm^{-1,}$ which were more visible in the synthesized compounds. The FTIR broad bands observed at 3438 and 3454 cm^{-1} are allocated to the stretching vibrations of the OH bond on the surface of clay-supported NCPs and CuO NPs respectively [77]. In contrast, the bands at 1632 and 1638 cm^{-1}

clay-supported CuO NCPs and CuO NPs have been endorsed to the adsorbed water molecules' O-H bending mode, respectively. In the same way, the C-H stretching bonds occur which came from ethanol solvent around in the region of 2930 and 2932 cm^{-1} for those of as-synthesized clay-supported CuO NCPs and CuO NPs [78]. The sample showed the most intensive band at 1109 cm^{-1} which was attributed to C-H bending vibration. The two obvious absorption peaks around 606 cm^{-1} and 516 cm^{-1} can be assigned to the vibrations of the copper (II) oxygen bonds in CuO NPs [79]. The vibrations about 605 cm^{-1} and 509 cm^{-1} were also assigned to Si–O–Si bond vibrations in clay-supported CuO NCPs.

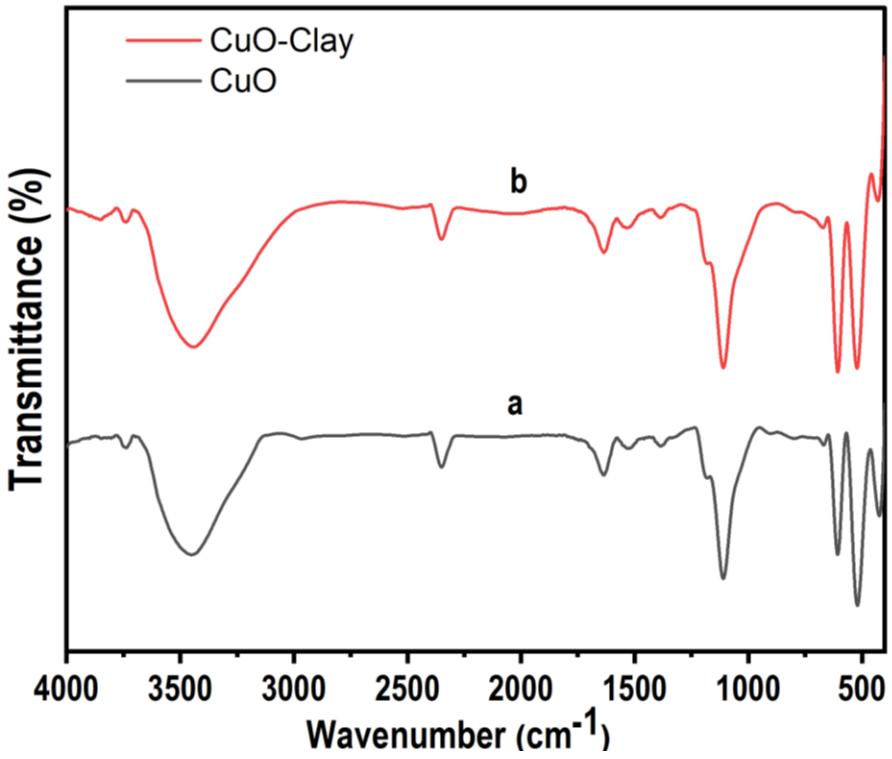

Figure 9: FT-IR spectrum of a) CuO and b) CuO clay-supported CuO NPs.

4.1.3. XRD Analysis

The crystalline nature and average crystal size of CuO NPs and Clay supported-CuO NCPs were confirmed by X-ray diffraction (XRD) analysis. As Figure 10 shows, the diffraction peaks observed in CuO NPs were at scattering angles (2θ) values of 16.61°, 22.89°, 35.61°, 38.83°, 48.83°, 61.57°, and 66.85° corresponding to the reflection from (220), (040), (111), (111),(202),

and (331) Whereas, the diffraction peaks observed in clay supported CuO NCPs at scattering angles (2θ) values of 35.59º, 38.86º, 48.65 º, 58.36º, 61.64º, 66.19º, and 68.23º corresponds to the reflection from (111), (111), (311), (110), (022), (202), and (331).

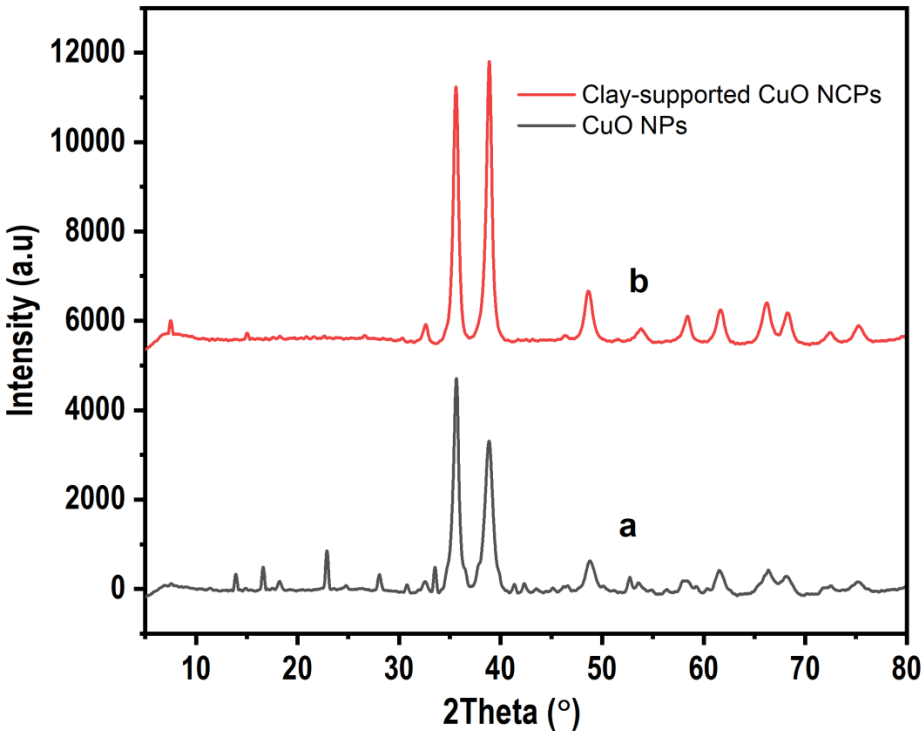

Figure 10: The XRD diffractograms of as-synthesized (a) CuO NPs and (b) clay-supported CuO NPCs.

The average crystallite sizes of the particles were calculated by using Debye-Scherer's equation as follows:

$$D = \frac{\kappa\lambda}{\beta cos\theta} \qquad (4.1)$$

Where D is the estimated crystal size in nanometer (nm) from XRD patterns, θ is the Bragg diffraction angle, λ is the X-ray wavelength (λ =0.15406 nm), β is the full width at the half maximum (FWHM) of the diffraction peak in radians and K is the shape factor or Scherrer constant (0.94) of Debye-Scherrer's equation.

Table 1: XRD analysis of numerical values and average size crystal (nm) of CuO NPs.

2θ(degree)	**2θ/2**	**(FWHM)**	**2θ/2 (radian)**	**β(radian)**	**crystal size(nm)**	**Average size (nm)**
16.61	8.306	0.263	0.145	0.00459	30.517	
22.89	11.445	0.292	0.199	0.00510	27.725	
35.61	17.806	0.711	0.311	0.0124	11.732	=10.06
38.83	19.415	1.005	0.338	0.0175	8.381	
48.83	24.41	0.979	0.426	0.0170	8.911	
61.57	30.788	0.784	0.537	0.0136	11.787	
66.85	33.423	2.338	0.583	0.0408	4.070	**Total =14.73**

Table 2: XRD analysis of numerical values and average size crystal (nm) of clay supported-CuO NCPs

2θ(degree)	**2θ/2**	**(FWHM)**	**θ(radian)**	**β(radian)**	**Crystal size (nm)**	**Average size (nm)**
35.59	17.796	0.648	0.3106	0.0113	12.866	
38.86	19.429	0.703	0.339	0.0122	11.975	
48.65	24.328	0.917	0.424	0.0160	9.501	=11.20
58.36	29.183	0.705	0.509	0.0123	12.898	
61.64	30.822	0.780	0.537	0.0136	11.847	
66.19	33.099	0.963	0.577	0.0168	9.847	
68.233	34.116	0.847	0.595	0.0147	11.328	**Total =11.466**

4.1.4. SEM analysis

The SEM was utilized to confirm the morphology, composition, and particle size of the as-synthesized samples using the JCM-6000 Plus SEM instrument. The synthesized clay-supported CuO NCPs and CuO NPs of average size were 11.466 and 14.732nm respectively, which corresponds to the nanoparticle size range. This variation in particle size supports XRD analysis in above Tables 1 and 2. The morphology of both CuO NPs and CuO NCPs were visible as presented in Figure 11 below. The SEM results of CuO NPs exhibit ellipsoidal morphology with various size ranges, A-E (3-50) µm. At higher magnifications, particularly at a 30-micrometer resolution, the images show a uniform and well-defined porous cavity structure. This porosity is crucial for holding nano-supportive samples effectively, as evidenced by the aggregated cavity structure. Additionally, the SEM images illustrate clay-supported CuO NCPs adopt a flower-like morphology, highlighting a distinct change in structure with various size ranges, F-I (1-10) µm and also those represented by a letter J at 500nm compared to compound CuO NPs. This morphology change is due to the presence of the nano clay sample in CuO NPs.

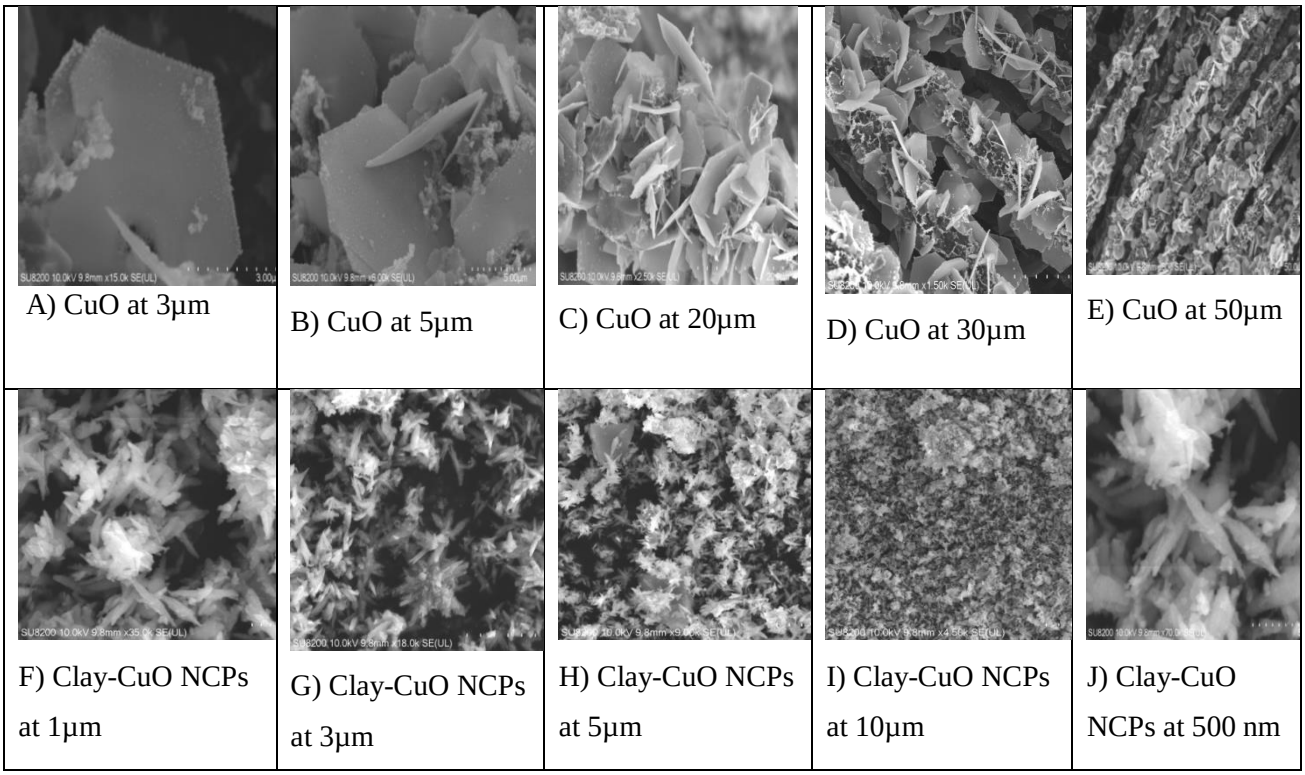

Figure 11: SEM image of CuO NPs in different size ranges, A-E (3, 5, 20, 30, and 50 µm) and similarly for clay-supported CuO NCPs in different size ranges F-I (1, 3, 5, and 10 µm), J (500nm)

4.1.5. EDX Analysis

The purity and elemental makeup of nanomaterials were assessed using EDX analysis. EDX result revealed that the sample contains elements of copper and oxygen confirming the formation of CuO NPs. The purity of synthesized CuO NPs was confirmed by the EDX spectrum as shown in below Table 3. Traces of sulfur have come from sulfate and carbon was attributed to ethanol compound solvent during the synthesis of CuO NPs. Repeated washing with distilled water can be done to eliminate the traces of surfer and carbon to obtain a pure sample. As shown in Table 3 below, the weight composition for copper and oxygen was 37.69% and 22.18% respectively. The atomic composition of copper and oxygen was then calculated as 11.27% and 26.34% respectively. CuO has a uniform distribution of copper and oxygen [80].

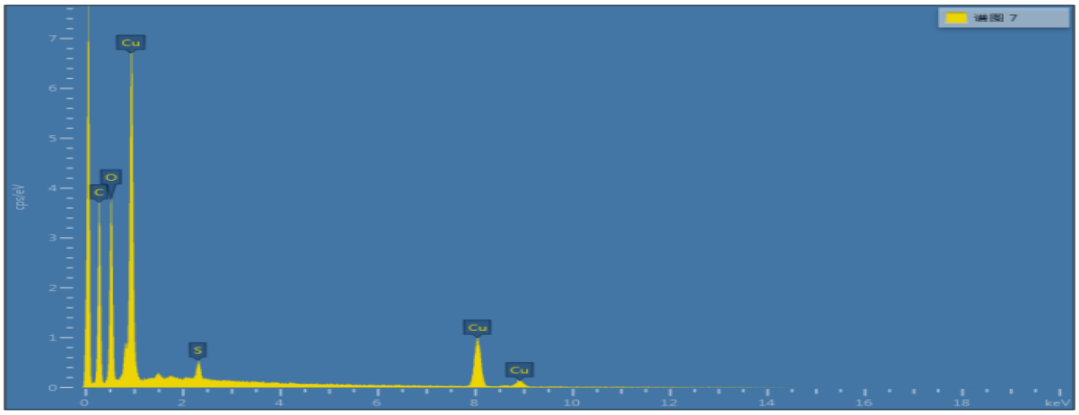

Figure 12: EDX spectrum of CuO NPs.

Table 3: EDX result of CuO NPs.

Elements	**Line type**	**Apparent Concentration**	**Wt%**	**Wt% Sigma**	**Atomic Percent**	**Standard Sample level**
C	K	10.01	39.03	0.38	61.74	C
O	K	17.88	22.18	0.27	26.34	SiO_2
S	K	0.95	1.11	0.06	0.66	FeS_2
Cu	L	20.95	37.69	0.34	11.27	Cu
Total			**100**		**100**	

As shown in Figure 13, the energy-dispersive X-ray spectroscopy (EDX) analysis also confirmed the presence of C, O, Mg, Si, Ca, Fe, and Cu as the main components of clay-supported CuO composites which indicate the formation of nanocomposites with respective elements.

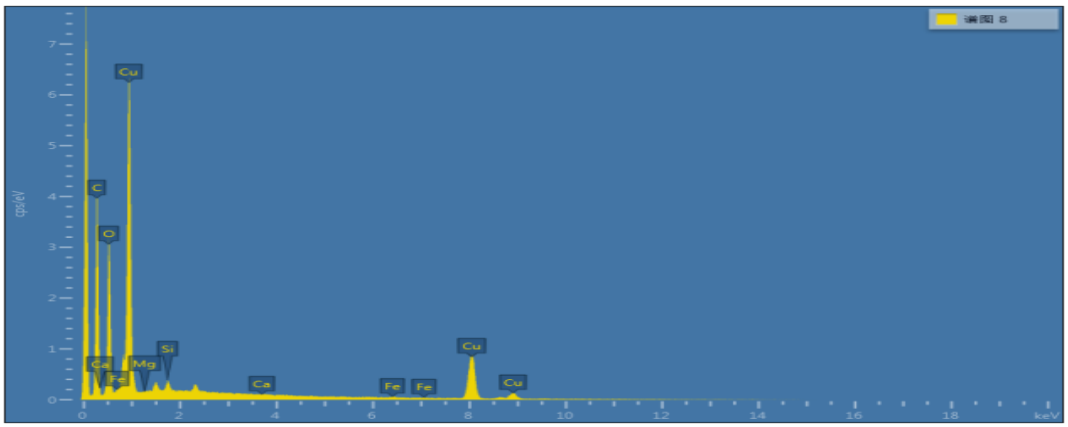

Figure 13: EDX spectrum of Clay supported-CuO NPs.

The weight composition and atomic composition of each of the respect elements are listed in Table 4 below.

Table 4: EDX result of clay-supported CuO NCPs

Elements	**Line type**	**Apparent Concentration**	**Wt%**	**Wt% Sigma**	**Atomic Percent**	**Standard Sample level**
C	K	11.11	41.92	0.34	65.05	C
O	K	15.35	20.27	0.23	23.61	SiO_2
Mg	K	0.04	0.08	0.05	0.06	MgO
Si	K	0.4	0.55	0.04	0.36	SiO_2
Ca	K	0.01	0.01	0.04	0.01	Wollastonite
Fe	K	0.24	0.32	0.1	0.11	Fe
Cu	L	20	36.85	0.29	10.81	Cu
Total			**100**		**100**	

4.2. Photocatalytic activity of synthesized CuO NPs and clay-supported CuO NCPs

4.2.1. Photocatalytic reaction setup.

For the photocatalytic degradation of Malachite green dye, we used a simple and inexpensive instrument setup consisting of a tungsten lamp, a cardboard box, and a stirrer as shown in Figure 14 below (A, B, and C) [81]. The cardboard box was used to house the sample solution and the catalyst (CuO NPs and clay-supported CuO NCPs), while the tungsten lamp was used as the light source for the photocatalytic process. The cardboard box was selected for its low cost and ease of handling. We prepared the box by cutting off one of its sides, leaving three sides and the bottom intact as shown in Figure 14B. This created a rectangular opening through which the light from the tungsten lamp could pass through and illuminate the sample solution. We placed the measured amount of CuO NPs and clay-supported CuO NCPs into the sample of dye solution and stirred the mixture to ensure uniform dispersion of the catalyst using a stirrer as shown in Figure 14C. The 200W tungsten lamp was purchased from Bahir Dar City. We chose a tungsten lamp for its relatively low cost and the availability of a wide range of wattage options. The lamp was placed at a distance of 30 cm from the sample solution. During the experiment, first, we placed the cardboard box with the sample solution and catalyst inside on a magnetic stirrer to ensure thorough mixing of the solution for adsorption-desorption takes place as shown in Figure 14D. The tungsten lamp was turned on and the solution was exposed to visible light for the desired duration as shown in Figure 14E. The temperature of the sample solution was monitored using a thermometer to ensure that it remained constant throughout the experiment. Overall, the setup of the photocatalytic instruments we used was simple, cost-effective, and easy to handle. By using a cardboard box and a tungsten lamp, we were able to create a functional photocatalytic system for the degradation of MG dye. While more sophisticated and expensive setups are available, our setup was suitable for our research objectives and provided reliable results.

A

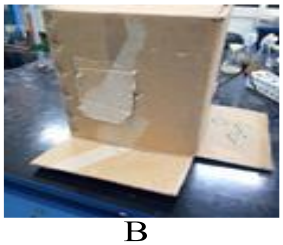

B

C

D

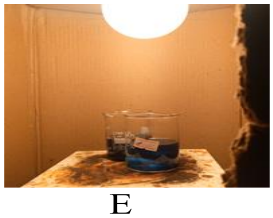

E

Figure 14: Photocatalytic instrumental setup and photocatalysis process in the photograph.

4.2.2. Photocatalytic degradation of MG dye using as-synthesized nanoparticles

The UV-Vis spectra of dye degradation of MG solution using CuO NPs and clay-supported CuO CNPs as a function of contact time as shown in Figures below 15(a) and 16(a). From the UV-Vis spectra, the wavelength range was measured at the range between 350 to 800 nm. At different time intervals, the absorbance measurements of MG solution were recorded at λmax =617 nm which is similar to a study done that reported a maximum wavelength of 620 nm [82]. A new peak appeared at around 425 nm which served as evidence for the destruction of MG dye molecules through photodegradation. It was observed that the absorbance of the dye solution decreased over time. The degradation at the initial stage was very rapid but no hypsochromic shift was seen in this spectrum. Thereafter, the dye degraded at a slow rate after adsorption throughout the whole photodegradation process. This is because the surface active sites of both catalysts were already occupied by dye molecules; hence the number of available free surface active sites of nanoparticles for the subsequent adsorption will be greatly reduced [83]. This will indirectly influence the rate of degradation because adsorption must happen first then followed by degradation of the dye molecules.

The overlapped absorption spectra of the MG within the synthesized catalysts were recorded at different time intervals over 180 min as indicated below in Figures 15(a) and 16(a). There was a gradual decrease in the intensity of the diagnostic peak of MG dye located at λ_{max} = 617 nm with an increase in the time of irradiation from 0 to 180 min. The photodegradation efficiency of the catalyst on MG dye was calculated using the relation in equation 3.4 above. The efficiency after 180 min of irradiation with UV light was 82.96 as revealed in Figure 15(b). The percentage degradation was calculated from the initial and final adsorption of the physical change that is associated with the degradation activity of the CuO NPs was the discoloration of the MG solution. While the degradation efficiency of MG dyes against clay-supported CuO NCPs was 89.67%, as revealed in Figure 16(b).

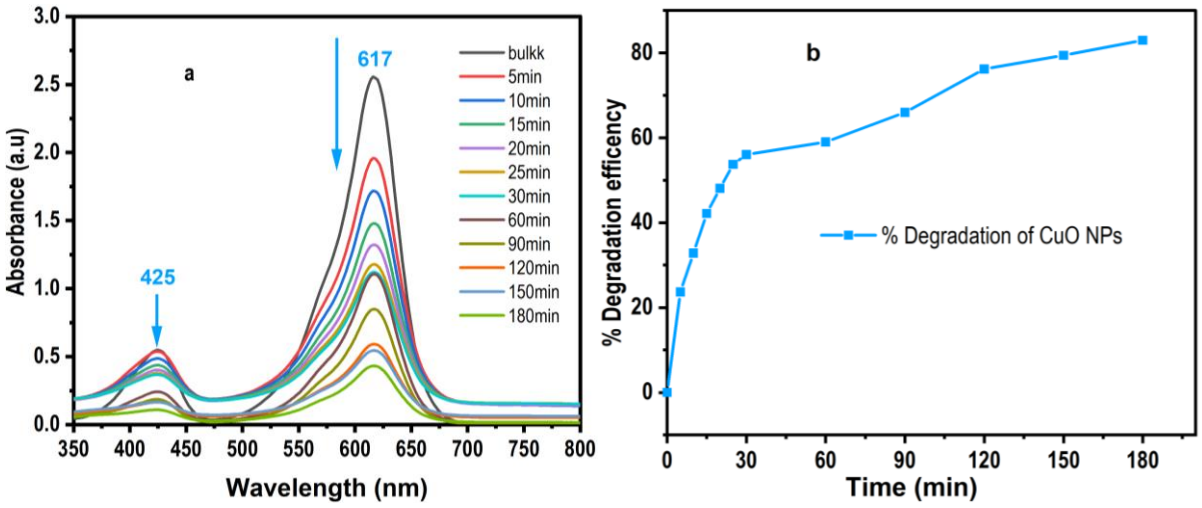

Figure 15: (a) Photocatalytic degradation of MG using CuO NPs as a catalyst and under UV irradiation and inset, (b) Spectra of percentage degradation.

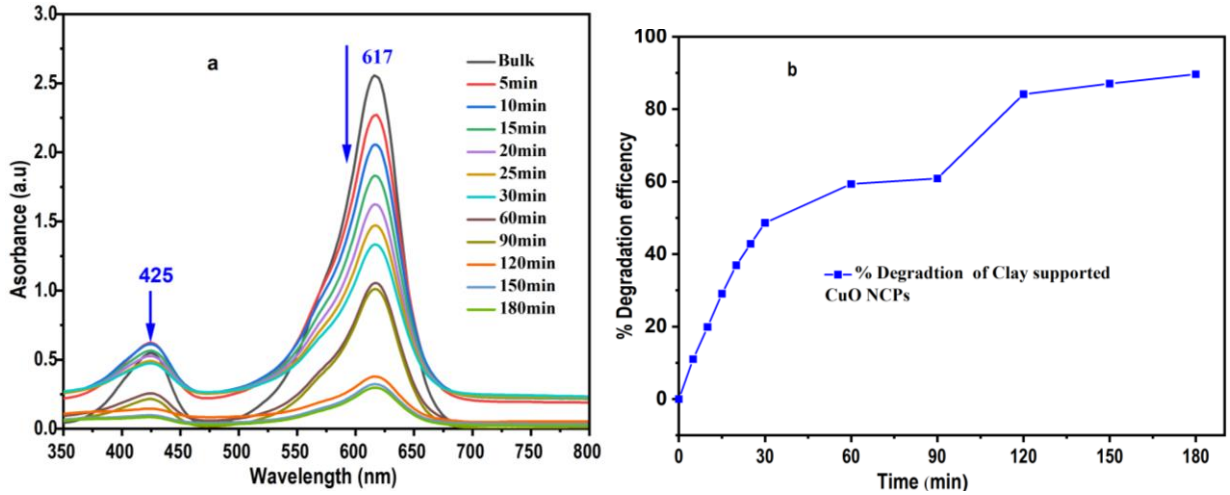

Figure 16: (a) Photocatalytic degradation of MG using clay-supported CuO NCPs as a catalyst and under UV irradiation and inset, (b) Spectra of percentage degradation.

The dye degradation was also visually monitored by the observation of a change in the color of the MG dye solution. The color of the dye was greenish-blue initially and that was slightly changed to a lighter green color after 30 min of applying the light bulb with catalyst. As the time of exposure to UV irradiation progressed to 180 min, there was a noticeable gradual change in color to different shades of light green. Ultimately, at 180 min it became more and more light green and this marked the degradation ability of MG dye solution using the synthesized CuO nanoparticles, as shown in Figure 17.

Figure 17: Photocatalytic degradation of MG dye using synthesized CuO NPs.

While using the as-synthesized clay-supported CuO NCPs, the dye degradation process was much higher than that of using a CuO nanoparticle catalyst. When we compared the degraded MG dye indicated in auto incubator test tubes as shown in Figures 17 and 18 at the same conditions, those containing clay-supported CuO NCPs catalyst as indicated in Figure 18 became more colorless. This indicated that the treatment of MG-containing wastewater in the photocatalyst process using Clay clay-supported CuO NCP catalyst is better than using a CuO NPs catalyst. It has been reported that the smaller the nanoparticle size, the better the efficiency of photocatalytic degradation of dyes [84].

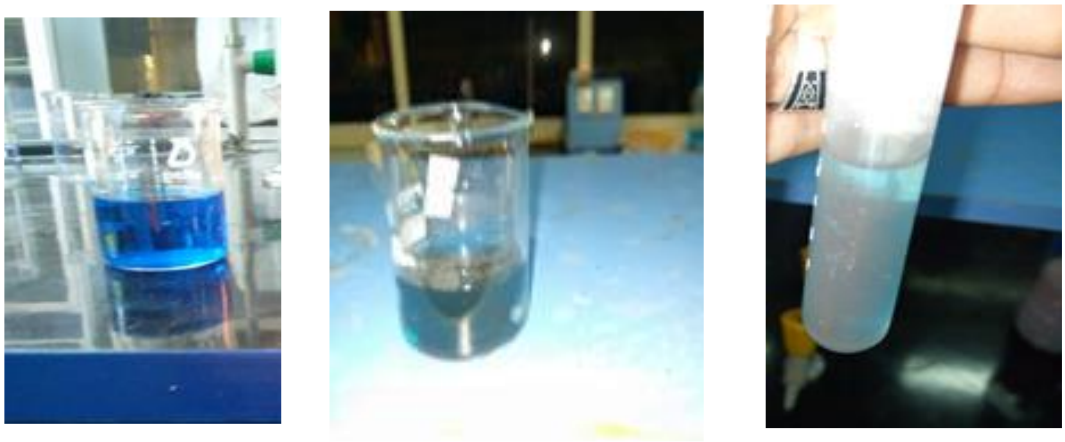

Figure 18: Photocatalytic degradation of MG dye using synthesized clay-supported CuO NCPs.

4.2.3. Photocatalytic Degradation Mechanism of MG Dye by Clay Supported CuO Nanocomposites.

The photogenerated hydroxyl radicals and superoxide radicals were responsible for the photocatalytic degradation of MG over clay-supported CuO NCPs. The proposed mechanism of the reaction is given: photocatalytic processes are usually triggered by irradiation of light as a result of photoelectrons increased from the valence band (VB) of the Clay/CuO catalyst to the conducting band (CB). This light that has been absorbed is now equal to or greater than the photocatalyst band gap energy (*E*g). The valence band developed a hole as a result of photoelectron excitation. Thus, as stated in the equation below, a pair of electrons and holes (e-/h+) are generated. The following equations (4.2) to (4.4) illustrate the photocatalytic reactions with carbon dioxide and water as the products of the degradation as reported in different studies [85].

$$\text{Clay/CuO} + hv \rightarrow \text{Clay/CuO}(e^-(CB) + h^+(VB)) \quad (4.2)$$

The formation of hydroxyl radicals, which occurs when water ionizes and reacts with the newly created hole in the valence band to produce a hydroxyl radical ($^{\bullet}OH$), is another process by which MG molecules degrade.

$$H_2O + h^+(VB) \rightarrow \dot{O}H(ads) + H^+(ads) \quad (4.3)$$

This Clay/CuO surface $OH^{\bullet}$ radical is a very potent oxidizing agent that attacks adsorbed MG molecules that are close to the catalyst surface and mineralized to the degree that depends on the structure and their stability non selectively. These hydroxyl radicals can kill any existing microorganisms in the medium in addition to attacking organic pollutants [86]. Similarly, the excited electrons in the conducting band now interact with the nearby oxygen to create anionic superoxide radical (O_2^-), as in equation 4.4.

$$O_2 + e^-CB \rightarrow O_2^-(ads) \quad (4.4)$$

These superoxide radicals aid in the oxidation process while also preventing the recombination of electrons and holes, keeping the Clay/CuO catalyst electron neutrality. Superoxide is protonated in this step, which results in the production of H_2O_2. During the prior step, superoxide ions were formed. These further dissociate and produce a hydroxyl radical, which is very volatile. The oxidation and reduction reactions occur concurrently on the photoexcited Clay/CuO catalyst surface in photocatalyst.

4.2.4. Kinetic Studies of Photocatalytic Degradation of MG dye

As shown in Figure 19 (a) below on the left side represents a plot of ln(Co/Ct) against time and the spectra showed a linear correlation against time. This displayed first-order kinetics of the photodegradation of MG dye using CuO NPs via light irradiation. The value of the correlation coefficient from the graph is 0.91428. Similarly, Figure 19 (b) on the right represents the plot of ln(Co/Ct) as a function of reaction time for the degradation of MG dye by using clay-supported CuO NCPs. Pseudo-first-order kinetics of photodegradation of MG dyes with a correlation coefficient of 0.9655 was obtained. Correlation coefficients in both cases have values close to 1 which revealed a good adsorption rate; however, clay-supported CuO NCPs catalyst yields better photocatalytic degradation products of MG dye effluent wastewater because of its higher Correlation coefficient value.

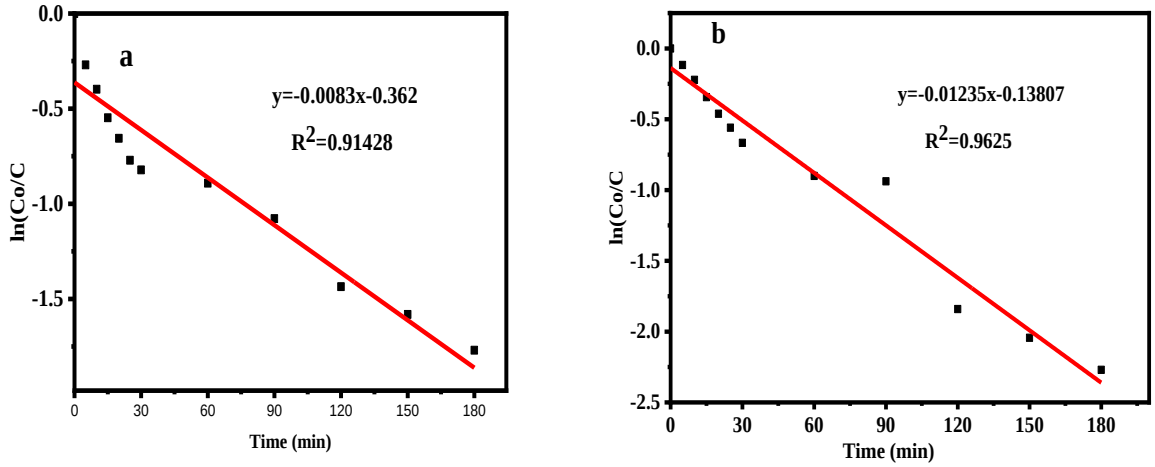

Figure 19: (a) Plot of lnCt/Co vs time for the first-order kinetics of photocatalytic degradation of MG dye using CuO NPs (b) using clay supported-CuO NCPs catalysts under UV light irradiation.

CHAPTER FIVE

5. CONCLUSION AND RECOMMENDATION

5.1. Summary and Conclusion

The clay-supported CuO NCPs have been synthesized through a co-precipitation method by employing $CuSO_4.5H_2O$ salt solution as a precursor. This method is effective for homogeneous dispersion clay suspension on metal salt solution conducted by the additive base environment to form clay deposited CuO. Different techniques were employed to characterize the synthesized NCPs such as X-ray diffraction, Fourier transforms infrared spectroscopy, ultraviolet/visible spectroscopy, SEM, EDX, and XRD that the NCPs crystalline in size (D = 11.466nm) which confirms nano size ranges. A Photocatalytic degradation property of the clay-supported CuO NCPs was evaluated by decomposing MG dye through the generation of reactive radical species with an easily available photocatalytic apparatus. The clay-supported CuO NCPs exhibited higher photocatalytic activity in the decomposition of MG under light irradiation and obtained almost about 89.67% degradation. The high efficiency of the clay-supported CuO composite was considered to be caused by the unique more active surface sites that are provided by clay during the synthesis of clay-supported CuO composites which help to the generation of more active radicals for the breakdown of organic contaminants by facilitating the separation of photogenerated electrons and holes. Also, the existence of Fe in clay-supported CuO NPS was not only to offer the site for the formation of the primary photocatalyst but also to engage in the electron transfer mechanism to avoid charge carrier recombination of CuO NPs in its photocatalytic process. Hence, clay in clay-supported CuO photocatalysts not only acts as a template to prevent the agglomeration and development of the major photocatalysts but also provides considerable suppression of charge recombination, which may prolong the lifetime of the electron-hole pair and enhance the degrading activity.

5.2. Recommendations

- Further research should be carried out through cyclic selection to synthesize clay-supported CuO NCPs by varying the clay ratio to a fixed amount of copper oxide or vice-verse to improve photocatalytic degradation dyes.
- The effect of parameters such as the amount of catalyst, concentration of substrate (dye) solution, pH, calcination temperature, and intensity of radiation on the photocatalytic degradation should be taken into account.
- The synthesized clay-supported CuO NCPs should be characterized by other techniques BET, TEM, etc.

REFERENCE

1. Yunusa, U., Usman, B., & Ibrahim, M. B. (2021). Cationic dyes removal from wastewater by adsorptive method: A systematic in-depth review. *Algerian Journal of Chemical Engineering AJCE*, 1(2), 6-40.
2. Saeed, M., Muneer, M., Haq, A. U., & Akram, N. (2022). Photocatalysis: An effective tool for photodegradation of dyes—A review. *Environmental Science and Pollution Research, 29(1), 293-3*11.
3. Bhatnagar, A., & Sillanpää, M. (2010). Utilization of agro-industrial and municipal waste materials as potential adsorbents for water treatment—a review. *Chemical Engineering Journal, 157(2-3), 277-296.*
4. Rafatullah, M., Sulaiman, O., Hashim, R., & Ahmad, A. (2010). Adsorption of methylene blue on low-cost adsorbents: a review. *Journal of hazardous materials, 177(1-3), 70-80.*
5. Velusamy, S., Roy, A., Sundaram, S., & Kumar Mallick, T. (2021). A review on heavy metal ions and containing dyes removal through graphene oxide-based adsorption strategies for textile wastewater treatment. *The Chemical Record*, *21*(7), 1570-1610.
6. Sarojini, G., Babu, S. V., Rajamohan, N., & Rajasimman, M. (2022). Performance evaluation of polymer-marine biomass-based nanocomposite for the adsorptive removal of malachite green from synthetic wastewater. *Environmental Research*, *204*, 112132.
7. Fabrication of sulfur-doped biochar derived from tapioca peel waste with superior adsorption performance for the removal of Malachite green and Rhodamine B dyes. *Surfaces and Interfaces*, *23*, 100920.
8. Rajesh, G., Kumar, P. S., Rangasamy, G., Akilandeswari, S., Mandal, A., Shankar, V. U., & Thirumalai, K. (2023). Fabrication of novel Ni-doped $CdAl_2O_4$ nanoparticles and applications in photo-oxidation processes under visible light illumination. *Molecular Catalysis*, *535*, 112835.
9. Anjum, M., Miandad, R., Waqas, M., Gehany, F., & Barakat, M. A. (2019). Remediation of wastewater using various nano-materials. *Arabian journal of chemistry*, 12(8), 4897-4919.

10. Dang, X., Huang, J., Cao, L., & Zhou, Y. (2013). Plasma-catalytic oxidation of adsorbed toluene with gas circulation. *Catalysis Communications*, 40, 116-119.
11. Wang, Q., & Astruc, D. (2019). State-of-the-art and prospects in metal-organic framework (MOF)-based and MOF-derived nanocatalysis. *Chemical Reviews*, *120*(2), 1438-1511.
12. Welderfael, T., Yadav, O. P., Taddesse, A. M., & Kaushal, J. (2013). Synthesis, characterization, and photocatalytic activities of Ag-N-codoped ZnO nanoparticles for degradation of methyl red. *Bulletin of the Chemical Society of Ethiopia*, 27(2), 221-232.
13. Badvi, K., & Javanbakht, V. (2021). Enhanced photocatalytic degradation of dye contaminants with TiO2 immobilized on ZSM-5 zeolite modified with nickel nanoparticles. *Journal of Cleaner Production*, *280*, 124518.
14. Rajabi, S. K., Sohrabnezhad, S., & Ghafourian, S. (2016). Fabrication of Fe_3O_4@ CuO core-shell from MOF-based materials and its antibacterial activity. *Journal of solid state chemistry*, *244*, 160-163.
15. Pirhashemi, M., & Habibi-Yangjeh, A. (2017). Ultrasonic-assisted preparation of plasmonic ZnO/Ag/Ag_2WO_4 nanocomposites with high visible-light photocatalytic performance for degradation of organic pollutants. *Journal of colloid and interface science*, *491*, 216-229.
16. Petronella, F., Truppi, A., Ingrosso, C., Placido, T., Striccoli, M., Curri, M. L., & Comparelli, R. (2017). Nanocomposite materials for photocatalytic degradation of pollutants. *Catalysis Today*, *281*, 85-100.
17. Selvaraj, V., Karthika, T. S., Mansiya, C., & Alagar, M. (2021). An over review of recently developed techniques, mechanisms, and intermediate involved in the advanced azo dye degradation for industrial applications. *Journal of molecular structure*, *1224*, 129195.
18. Zhang, S., Wang, J., Zhang, Y., Ma, J., Huang, L., Yu, S., Chen, L., Song, G., Qiu, M., Wang, X., 2021. Applications of water-stable metal-organic frameworks in the removal of water pollutants: *A review. Environmental Pollution*.

19. Wang, Y., Lany, S., Ghanbaja, J., Fagot-Revurat, Y., Chen, Y., Soldera, F., Horwat, D., Mücklich, F., Pierson, J., 2016. Electronic structures of Cu_2O, Cu_4O_3, and CuO: A joint experimental and theoretical study. *Physical Review*

20. Ighalo, J.O., Sagboye, P.A., Umenweke, G., Ajala, O.J., Omoarukhe, F.O., Adeyanju, C.A., Ogunniyi, S., Adeniyi, A.G., 2021. CuO nanoparticles (CuO NPs) for water treatment: A review of recent advances. *Environmental Nanotechnology, Monitoring & Management.*

21. Xu, C., Anusuyadevi, P. R., Aymonier, C., Luque, R., & Marre, S. (2019). Nanostructured materials for photocatalysis. *Chemical Society Reviews*, *48*(14), 3868-3902.

22. Wang, J., & Wang, S. (2022). A critical review on graphitic carbon nitride (g-C_3N_4)-based materials: Preparation, modification and environmental application. *Coordination Chemistry Reviews,* 453, 214338.

23. Li, C., Sun, Z., Zhang, W., Yu, C., & Zheng, S. (2018). Highly efficient g-C_3N_4/TiO_2/kaolinite composite with novel three-dimensional structure and enhanced visible light responding ability towards ciprofloxacin and S. aureus. *Applied Catalysis B: Environmental*, *220*, 272-282.

24. Nazeri, M. T., Nasiriani, T., Torabi, S., & Shaabani, A. (2024). Isocyanide-based multicomponent reactions for the synthesis of benzopyran derivatives with biological scaffolds. *Organic & Biomolecular Chemistry*, *22*(6), 1102-1134.

25. Qiu, M., Liu, L., Ling, Q., Cai, Y., Yu, S., Wang, S., & Wang, X. (2022). Biochar for the removal of contaminants from soil and water: *a review. Biochar,* 4(1), 19.

26. Groiss, S., Selvaraj, R., Varadavenkatesan, T., & Vinayagam, R. (2017). Structural characterization, the antibacterial and catalytic effect of iron oxide nanoparticles synthesized using the leaf extract of Cynometra ramiflora. *Journal of Molecular Structure*, *1128*, 572-578.

27. Fang, M., Tan, X., Liu, Z., Hu, B., Wang, X., 2021. Recent progress on metal-enhanced photocatalysis: a review on the mechanism. *Research* 2021, 1-16.

28. Sharma, K., Dutta, V., Sharma, S., Raizada, P., Hosseini-Bandegharaei, A., Thakur, P., Singh, P., 2019. Recent advances in enhanced photocatalytic activity of bismuth oxyhalides for efficient photocatalysis of organic pollutants in water: A review. *Journal of Industrial and Engineering Chemistry* 78, 1-20.

29. S. Roy, T. K. Das (2015). Plant Mediated Green Synthesis of Silver Nanoparticles-A Review. *International Journal of Plant Biology & Research, 3(3), 1 - 11.*
30. A.R. Shet, P. Ghose, L. Patil, V. Hombalimath (2015). A preliminary study on green synthesis and antibacterial activity of silver nanoparticles. *International Journal of Current Biotechnology*, 3(2), 1-6.
31. N. Sundaramurthy, C. Parthiban (2015). Biosynthesis of copper oxide nanoparticles using Pyrus Pyrifolia leaf extract and evolving the catalytic activity. *International Research Journal of Engineering and Technology (IRJET)*, 2(6), 332-338.
32. M. Thamilselvan (2012). Antibacterial activity of Cu_2O nanoparticles on E.Colisynthesized from Tridax procumbens leaf extract and surface. *Journal of Nanomaterials and Biostructures,* 7(2), 833 - 839.
33. H. Sylvia Devi, T.D. Singh (2014). Synthesis of Copper Oxide nanoparticles by a novel method and its application in the degradation of Methyl Orange. *Advance inElectronic and Electric Engineering*, 4(1), 83-88.
34. G. Ren, D. Hu, E.W.C. Cheng, M. A. Vargas-Reus, P. Reip, R.P. Allaker (2009). Characterization of copper oxide nanoparticles for antimicrobial applications. *International Journal of Antimicrobial Agents*, 33(6), 587- 590.
35. Waris, A., Din, M., Ali, A., Ali, M., Afridi, S., Baset, A., & Khan, A. U. (2021). A comprehensive review of green synthesis of copper oxide nanoparticles and their diverse biomedical applications. *Inorganic Chemistry Communications*, 123, 108369.
36. Katowah, D. F., Saleh, S. M., Alqarni, S. A., Ali, R., Mohammed, G. I., & Hussein, M. A. (2021). Network structure-based decorated CPA@ CuO hybrid nanocomposite for methyl orange environmental remediation. *Scientific reports*, *11*(1), 5056.
37. Naz, S., Gul, A., Zia, M., & Javed, R. (2023). Synthesis, biomedical applications, and toxicity of CuO nanoparticles. Applied Microbiology and Biotechnology, 107(4), 1039-1061.
38. Araújo, E. S., Pereira, M. F., da Silva, G. M., Tavares, G. F., Oliveira, C. Y., & Faia, P. M. (2023). A Review on the Use of Metal Oxide-Based Nanocomposites for the Remediation of Organics-Contaminated Water via Photocatalysis: Fundamentals, Bibliometric Study and Recent Advances. Toxics, 11(8), 658.

39. Védrine, J. C. (2019). Metal oxides in heterogeneous oxidation catalysis: State of the art and challenges for a more sustainable world. *Chem Sus Chem*, 12(3), 577-588.
40. Bogale, B., Asere, T. G., Yai, T., & Melak, F. (2023). Photocatalytic degradation of methylene blue dye using cuprous oxide/graphene nanocomposite. *Current Nanomaterials*, 8(2), 182-193.
41. Dey, A. (2018). Semiconductor metal oxide gas sensors: *A review. Materials Science and Engineering*: B, 229, 206-217.
42. Mulik, S. V., Dhas, S. D., Moholkar, A. V., Parale, V. G., Park, H. H., Koyale, P. A., & Delekar, S. D. (2023). Square-facet nano bar MOF-derived Co_3O_4@ Co/N-doped CNT core–shell-based nanocomposites as cathode materials for high-performance supercapacitor studies. *ACS omega*, 8(2), 2183-2196.
43. Alshangiti, D. M., El-Damhougy, T. K., Zaher, A., & Madani, M. (2023). Revolutionizing biomedicine: Advancements, applications, and prospects of nanocomposite macromolecular carbohydrate-based hydrogel biomaterials: *A review. RSC advances, 13(50), 35251-35291.*
44. P. Mallick, S. Sahu (2012). Structure, microstructure, and optical absorption analysis of CuO nanoparticles synthesized by sol-gel route. *Nanoscience and Nanotechnology, 2(3), 71-74.*
45. Ashrafi, G., Nasrollahzadeh, M., Jaleh, B., Sajjadi, M., & Ghafuri, H. (2022). Biowaste-and nature-derived (nano) materials: Biosynthesis, stability and environmental applications. *Advances in Colloid and Interface Science*, *301*, 102599.
46. Fatimah, I., Fadillah, G., Yanti, I., & Doong, R. A. (2022). Clay-supported metal oxide nanoparticles catalytic advanced oxidation processes: a review. *Nanomaterials*, *12*(5), 825.
47. Cecilia, J. A., García-Sancho, C., Vilarrasa-García, E., Jiménez-Jiménez, J., & Rodriguez-Castellón, E. (2018). Synthesis, characterization, uses and applications of porous clays heterostructures: a review. *The Chemical Record*, *18*(7-8), 1085-1104.
48. Chang, J., Ma, J., Ma, Q., Zhang, D., Qiao, N., Hu, M., & Ma, H. (2016). Adsorption of methylene blue onto Fe_3O_4/activated montmorillonite nanocomposite. *Applied Clay Science*, *119*, 132-140.

49. Kashif, M., Yuan, M., Su, Y., Heynderickx, P. M., & Memon, A. (2023). A review on pillared clay-based catalysts for low-temperature selective catalytic reduction of NOx with hydrocarbons. *Applied Clay Science*, *233*, 106847.

50. Zhang, M. H., Dong, H., Zhao, L., Wang, D. X., & Meng, D. (2019). A review of the Fenton process for organic wastewater treatment based on an optimization perspective. *Science of the Total Environment*, *670*, 110-121.

51. Yang, Y., Wang, X., Yang, F., Mu, B., & Wang, A. (2023). Progress and prospects of hemostatic materials based on nanostructured clay minerals. *Biomaterials science*, *11*(23), 7469-7488.

52. Ma, Y., Wang, X., Jia, Y., Chen, X., Han, H., & Li, C. (2014). Titanium dioxide-based nanomaterials for photocatalytic fuel generations. *Chemical Reviews*, *114*(19), 9987-10043.

53. Wang, J., Farias, J., Tiwary, A., Tangyie, G. C., & Huddersman, K. (2022). Advance Oxidation Process (AOP) of Bisphenol A Using a Novel Surface-Functionalised Polyacrylonitrile (PAN) Fibre Catalyst. *Water*, *14*(4), 640.

54. Daneshvar, N., Salari, D., & Khataee, A. R. (2004). Photocatalytic degradation of azo dye acid red 14 in water on ZnO as an alternative catalyst to TiO_2. Journal of photochemistry and photobiology A: *Chemistry*, 162(2-3), 317-322.

55. Altun, E. Y., ŞİŞMANOĞLU, Z. T., & Soylu, G. S. P. (2021). Photocatalytic decomposition of textile dyestuffs by photosensitive metal oxide catalysts. *Turkish Journal of Chemistry*, 45(5), 1432-1443.

56. Nagarajan, D., Kusmayadi, A., Yen, H. W., Dong, C. D., Lee, D. J., & Chang, J. S. (2019). Current advances in biological swine wastewater treatment using microalgae-based processes. *Bioresource Technology*, 289, 121718.

57. Ameen, S., Murtaza, M., Arshad, M., Alhodaib, A., & Waseem, A. (2022). Perovskite LaNiO3/Ag3PO4 heterojunction photocatalyst for the degradation of dyes. *Frontiers in Chemistry*, 10, 969698.

58. Ghanbari, F., & Moradi, M. (2017). Application of peroxymonosulfate and its activation methods for degradation of environmental organic pollutants. *Chemical Engineering Journal*, 310, 41-62.

59. Hao, O. J., Kim, H., & Chiang, P. C. (2000). Decolorization of wastewater. *Critical reviews in environmental science and technology*, 30(4), 449-505.

60. Zhang, J., Feng, L., Wei, J., Guo, X., & Cao, W. (2006). Synthesis of SnO_2/TiO_2 nanocomposite photocatalysts by supercritical fluid combination technology. *Chinese Science Bulletin*, 51, 2050-2054.

61. Chen, H., Lee, S. W., Kim, T. H., & Hur, B. Y. (2006). Photocatalytic decomposition of benzene with plasma sprayed TiO2-based coatings on foamed aluminum. *Journal of the European Ceramic Society*, 26(12), 2231-2239.

62. Low, J., Yu, J., Jaroniec, M., Wageh, S., & Al-Ghamdi, A. A. (2017). Heterojunction photocatalysts. *Advanced materials*, *29*(20), 1601694.

63. Li, G., & Gray, K. A. (2007). The solid-solid interface: Explaining the high and unique photocatalytic reactivity of TiO_2-based nanocomposite materials. *Chemical physics*, *339*(1-3), 173-187.

64. Mishra, A., Mehta, A., & Basu, S. (2018). Clay supported TiO_2 nanoparticles for photocatalytic degradation of environmental pollutants: *A review. Journal of Environmental Chemical Engineering*, *6*(5), 6088-6107.

65. Park, H., Kim, H. I., Moon, G. H., & Choi, W. (2016). Photoinduced charge transfer processes in solar photocatalysis based on modified TiO_2. *Energy & Environmental Science*, *9*(2), 411-433.

66. Singh, J., Kumari, P., & Basu, S. (2019). Degradation of toxic industrial dyes using SnO2/g-C3N4 nanocomposites: role of mass ratio on photocatalytic activity. *Journal of Photochemistry and Photobiology A: Chemistry*, *371*, 136-143.

67. Hosseini, F., Kasaeian, A., Pourfayaz, F., Sheikhpour, M., & Wen, D. (2018). Novel ZnO-Ag/MWCNT nanocomposite for the photocatalytic degradation of phenol. *Materials Science in Semiconductor Processing*, *83*, 175-185

68. Logita, H. H., Tadesse, A., & Kebede, T. (2015). Synthesis, characterization, and photocatalytic activity of $MnO_2/Al_2O_3/Fe_2O_3$ nanocomposite for degradation of malachite green. *African Journal of Pure and Applied Chemistry*, 9(11), 211-222.

69. Singh, A., Singh, N. B., Hussain, I., Singh, H., & Yadav, V. (2017). Synthesis and characterization of copper oxide nanoparticles and their impact on germination of Vigna radiata (L.) R. Wilczek. *Tropical Plant Research*, *4*(2), 246-253.

70. Loosli, F., Yi, Z., Wang, J., & Baalousha, M. (2019). Improved extraction efficiency of natural nanomaterials in soils to facilitate their characterization using a multi-method approach. *Science of the Total Environment*, 677, 34-46.
71. Zhu, T. T., Zhou, C. H., Kabwe, F. B., Wu, Q. Q., Li, C. S., & Zhang, J. R. (2019). Exfoliation of montmorillonite and related properties of clay/polymer nanocomposites. *Applied clay science*, 169, 48-66.
72. Mourdikoudis, S., Pallares, R. M., & Thanh, N. T. K.Characterization techniques for nanoparticles: Comparison and complementarity upon studying nanoparticle properties. *Nanoscale*, 10(27), 12871–12934, 2018.
73. Khan, S. A., Khan, S. B., Khan, L. U., Farooq, A., Akhtar, K., & Asiri, A. M. Fourier transform infrared spectroscopy: Fundamentals and application in functional groups and nanomaterials characterization. *Handbook of Materials Characterization*, 317–344, 2018.
74. Xu, C., L. Cao, G. Su, W. Liu, X. Qu, and Y. Yu, 2010. Preparation characterization and photocatalytic activity of Co-doped ZnO powders. J. Alloys Compd. 497: 373–376.
75. Hong, R.Y., J.H. Li, L.L. Chen, D.Q. Liu, H.Z. Li, Y. Zheng and J. Ding, 2009. Synthesis, surface modification, and photocatalytic properties of ZnO nanoparticles. Powd. *Techno*. 189: 426–432.
76. ShilpaMolakkalu Padre, S. Kiruthika, ShridharMundinamani, Ravikirana, SrivathsavaSurabhi, Jong-RyulJeong, Kunabevu Mallikarjunappa Eshwarappa, Mudiyaru Subrahmanya Murari, Vignesh Shetty, Mamatha Ballal, and Gurumurthy S. C.(2022). Mono- and Bimetallic Nanoparticles for Catalytic Degradation of Hazardous Organic Dyes and Antibacterial Applications. *ACS. Omega*, 7, 35023−35034.
77. Bouafia, A., & Laouini, S. E. (2020). Green synthesis of iron oxide nanoparticles by aqueous leaves extract of Mentha Pulegium L.: Effect of ferric chloride concentration on the type of product. *Materials Letters*, *265*, 127364.
78. Xu, Y. Y., Bian, C., Chen, S., & Xia, S. (2006). A microelectronic technology-based amperometric immune sensor for α-fetoprotein using mixed self-assembled monolayers and gold nanoparticles. *Analytica chimica acta*, *561*(1-2), 48-54.

79. Chabri, S., Dhara, A., Show, B., Adak, D., Sinha, A., & Mukherjee, N. (2016). Mesoporous CuO-ZnO p-n hetero junction-based nanocomposites with high specific surface area for enhanced photocatalysis and electrochemical sensing. *Catalysis Science & Technology*, 6(9), 3238-32

80. Pouthika, K., & Madhumitha, G. (2024). Design and development of Carissa edulis fruit extract mediated bimetallic CuO-NiO-HNT composites for photocatalytic removal of food dye and antibiotic drug. *Journal of Molecular Structure*, 1295, 136665.

81. Kebede, M. A., Wubieneh, T. A., Yohannes, Y. B., & Shah, K. J. (2023). Green synthesis of zinc oxide from aqueous fruit extract of Dovyalis abyssinica (Koshem) and application for water purification. *Ethiopian Journal of Science and Technology*, *16*(1), 1-12.

82. Ameta, K., Tak, P., Soni, D. and Ameta, S. C., 2014. Photocatalytic decomposition of malachite green over lead chromate powder. *Scientific Reviews & Chemical Communications*, 4(1), pp. 38-45.

83. Movahedi, M., Mahjoub, A. R. and Janitabar-Darzi, S., 2009. Photodegradation of Congo Red in aqueous solution on ZnO as an alternative catalyst to TiO_2. *Journal of the Iranian Chemical Society*, 6(3), pp. 570-577.

84. Raliya, R., Avery, C., Chakrabarti, S., & Biswas, P. (2017). Photocatalytic degradation of methyl orange dye by pristine titanium dioxide, zinc oxide, and graphene oxide nanostructures and their composites under visible light irradiation. *Applied Nanoscience*, *7*, 253-259.

85. Yang, C.; Dong, W.; Cui, G.; Zhao, Y.; Shi, X.; Xia, X.; Tang, B.; Weiliang, W. Highly Efficient Photocatalytic Degradation of Methylene Blue by P2ABSA-Modified TiO_2 Nanocomposite Due to the Photosensitization Synergetic Effect of TiO_2 and P2ABSA. *RSC, Adv.* 2017, 7, 23699–23708.

86. Ajmal, A., Majeed, I., Malik, R. N., Idriss, H., & Nadeem, M. A. (2014). Principles and mechanisms of photocatalytic dye degradation on TiO_2 based photocatalysts: a comparative overview. *RSC Advances*, *4*(70), 37003-37026.